Journal of Molecular Liquids 385 (2023) 122385

Contents lists available at ScienceDirect

Journal of Molecular Liquids

journal homepage: www.elsevier.com/locate/molliq

Heat transfer characteristics of fluids containing paraffin core-metallic shell nanoencapsulated phase change materials for advanced thermal energy conversion and storage applications

Oguzhan Kazaz [a], Nader Karimi [a,b], Shanmugam Kumar [a], Gioia Falcone [a], Manosh C. Paul [a,*]

[a] Systems, Power & Energy Research Division, James Watt School of Engineering, University of Glasgow, Glasgow G12 8QQ, UK
[b] School of Engineering and Materials Science, Queen Mary University of London, London E1 4NS, UK

ARTICLE INFO

Keywords:
Phase change material
Nanoencapsulation
Solar energy
Phase change slurry
Photothermal conversion and storage
Surface plasmon resonance effect

ABSTRACT

The influence of heat transfer characteristics of fluids filled with paraffin core-metallic shell nanoencapsulated phase change material (PCM) on photothermal conversion and storage in a volumetrically heated solar system is numerically analysed. The results show that nanoencapsulated paraffin/Al, paraffin/Au, paraffin/Ag, and paraffin/Cu filled heat transfer fluids enhance the energy storage by 68, 73, 92 and 86 %, respectively as compared with the water-based Al, Au, Ag and Cu nanofluids. It is found that the phase change slurry (PCS) improves the temperature and storage gain, as the utilization of nanoencapsulated PCM and the rise in PCM mass concentration enhance the solar energy absorption power of the slurry. The maximum enhancement in stored energy is also observed for paraffin/Cu PCM filled slurry for a particle diameter of 15 nm. The enhancement in mass concentration of paraffin from 5 to 20 %, improves the thermal performance from 312 to 554 % compared to pure water, respectively. Increasing the size of the core/shell architecture of the PCM, however, reduces the surface area-to-volume ratio of the capsule, causing aggregation of the particles and decreasing the heat transfer between the capsule and the host fluid. This in turn results in decrease in temperature gain. Furthermore, it is noticed that the merger of mono- and hybrid- nanoparticles augments the thermal performance of the PCS. The findings of the study indicate that the paraffin core-metallic shell nanoencapsulated PCMs would significantly enhance the performance of advanced photothermal energy conversion and storage devices.

1. Introduction

The harms of fossil fuels to the environment, the increase in their prices and their depletion have revealed the importance of utilizing alternative energy sources [1,2,3]. Therefore, the use of decarbonizing technologies contributes to both the reduction of global temperature rise and carbon emissions by reducing the dependence on fossil fuels [4,5]. These technologies [6], if used in sustainable energy production, will contribute to reducing carbon emissions. Renewable energy is increasing in use because it is obtained from environmentally friendly and natural resources.

Today, solar energy contributes a significant share to environmentally friendly and sustainable energy and will continue to do so by reducing carbon dioxide emissions [7]. Sunlight must be caught, however, to benefit from the abundant solar energy, surface-based solar collectors (SBSCs), also known as conventional solar collectors that capture sunlight through the absorption plate and transfer it to the heat transfer fluid are desired. Since the temperature variation between the absorption plate and the working fluid is high, the collector efficiency is usually low [8]. To overcome this limitation, however, direct absorption solar collectors (DASCs) that can absorb the solar irradiation directly using the working fluid are employed [9]. The DASCs can improve the collector efficiency by reducing the temperature variation [10].

Nanoparticles can be added to the host fluid [11] and employed [12] as a heat transfer medium to increase the thermal performance of DASCs [13,14]. Zeiny et al. [15] experimentally examined the thermal behaviour of the water based fluids containing various nanoparticles such as carbon black, gold-copper hybrid, copper, and gold. The results demonstrated that hybrid nanoparticles did not enhance the solar conversion efficiency due to the particle fraction's dilution. Carbon black nanofluid was found to be the best among them due to its cost and efficiency. The experimental and numerical study of Jin et al. [16] analysed the influence of thermal performance of water based gold

* Corresponding author.
E-mail address: Manosh.Paul@glasgow.ac.uk (M.C. Paul).

https://doi.org/10.1016/j.molliq.2023.122385
Received 5 May 2023; Received in revised form 5 June 2023; Accepted 16 June 2023
Available online 17 June 2023

Nomenclature

I_λ	Radiation intensity (W/m^{2}μm)
k	Absorption index
$K_{a\lambda}$	Absorption coefficient (1/m)
$\overrightarrow{s}'$	Scattering direction vector
N_T	Particle number in unit volume
α	Polarizability
R	Effective mean free path
τ_{bulk}	Bulk metal free electron scattering time
$I_{b\lambda}$	Black body intensity (W/m^{2}μm)
$K_{e\lambda}$	Extinction coefficient (1/m)
r	Radius
T	Temperature (K)
C_{abs}	Absorption cross sections (cm^2)
l_∞	Bulk free electron mean free path
E	Enhancement
$\overrightarrow{s}$	Direction vector
P	Ratio of shell volume to total particle volume
q	Heat (J/kg)
C_p	Specific heat (J/kgK)
c_m	Mass concentration
d	Diameter
Q_{sca}	Scattering efficiency of core/shell
k	Thermal conductivity (W/mK)
$\gamma(R)$	Scattering rate
H	Latent heat of fusion (J/kg)
FVM	Finite volume method
p	Pressure (Pa)
y	Core-shell weight ratio
T_0	Initial temperature (K)
V_f	Fermi velocity
ΔH	Total enthalpy change (J/kg)
Gr	Grashof number
C_{sca}	Scattering cross sections (cm^2)
Ste	Stefan number
$\overrightarrow{r}$	Position vector
Q_{abs}	Absorption efficiency of core/shell
h	Convective heat transfer coefficient
c_v	Volume concentration
α_λ	Spectral absorption coefficient (1/m)
γ_∞	Inverse of the bulk relaxation time
n	Refractive index
u, v	Velocity vectors (m/s)
σ_s	Scattering coefficient (1/m)
g	Gravitational acceleration (m/s^2)
Pr	Prandtl number
A	Geometric parameter
w_p	Bulk plasma frequency
C_{ext}	Extinction cross sections (cm^2)
Re	Reynolds number
PCS	Phase change slurry
q''	Heat flux (W/m^2)
PCM	Phase change material

Greek symbols

Ω'	Solid angle
ρ	Density (kg/m^3)
σ	Stefan-Boltzmann (5.67×10^{-8} W/m^{2}K^4)
μ	Dynamic viscosity (Ns/m^2)
λ	Wavelength of incident light (μm)
Φ	Dissipation functions
β	Thermal expansion coefficient (1/K)
Φ	Phase function
ε	Emissivity

Subscripts

s	Shell
f	Base fluid
b	Slurry
p	Particle
1	Solidus
2	Liquidus
r	Radiative
amb	Ambient
c	Core

nanofluid. They developed a theoretical model, which was utilized for the prediction of absorption efficiency. It was realized that the temperature difference of the nanofluid enhanced with increasing particle concentration. Further, it was declared that the photothermal conversion efficiency of gold nanofluids reached 76 % at 5.8 ppm concentration. Lenert and Wang [17] conducted experimental research for the optimization of the collector based on the carbon-coated absorbing nanoparticles dispersed in Therminol VP-1. The influence of nanofluid height, radiative intensity and optical thickness were tested through a one dimensional heat transfer model. As the solar radiation and nanofluid height improved, the receiver efficiency was found to increase. When the receiver was connected to a power loop and the optical thickness and radiation time were optimized, the receiver side efficiency was estimated to be higher than 35 %.

An issue associated with solar energy is the inability to benefit from sunlight for 24 h. Therefore, it is desired to use the thermal energy obtained from the conversion of solar radiation during night-time [18]. Thanks to this storage of thermal energy, it can simultaneously meet heating, storage, and energy demands [18]. For this, PCMs that can store/release high latent heat during the phase change are utilised [19]. Due to these advantages of PCMs [20], their usage in different types of solar collectors is increasing [21]. Charvát et al. [22] experimentally and numerically analysed the paraffin based PCM flat plate solar collector to analyse the impact of latent thermal energy storage. They constructed two different solar collectors; the one had a sheet metal based absorber plate and the other one had PCM based aluminium panels. The results indicated that the peak-to-peak amplitudes of the outlet temperature of the fluid diminished from 284.15 °C to 278.15 °C when PCM was employed. They revealed that when the fluid temperature increased along the absorber plate, it could be more appropriate to apply PCMs with different phase transition temperatures. Essa et al. [23] compared the thermal performances of a two fins U-tube direct flow collector with and without PCM by varying flow rates (0.25, 0.35, and 1.2 LPM). The experimental results revealed that the PCM was melted, and the maximum efficiency at low flow rates was noted. Although the phase change transition was not completed as the flow rates increased, the useful heat and system efficiency improved. A numerical investigation was employed to study the influence of combined PCM on photovoltaic thermal system by Kazemian et al. [24]. The effect of thermal conductivity and enthalpy of fusion of PCM, melting temperature, mass flow rate and solar radiation were investigated. It was found that the surface and cooler outlet temperatures of the photovoltaic thermal system integrated with PCM were lower than the system without PCM. The electrical and thermal efficiencies improved by 1.34 % and 6.59 %, respectively when the thermal conductivity was augmented from 0.1 W/mK to 0.5 W/mK.

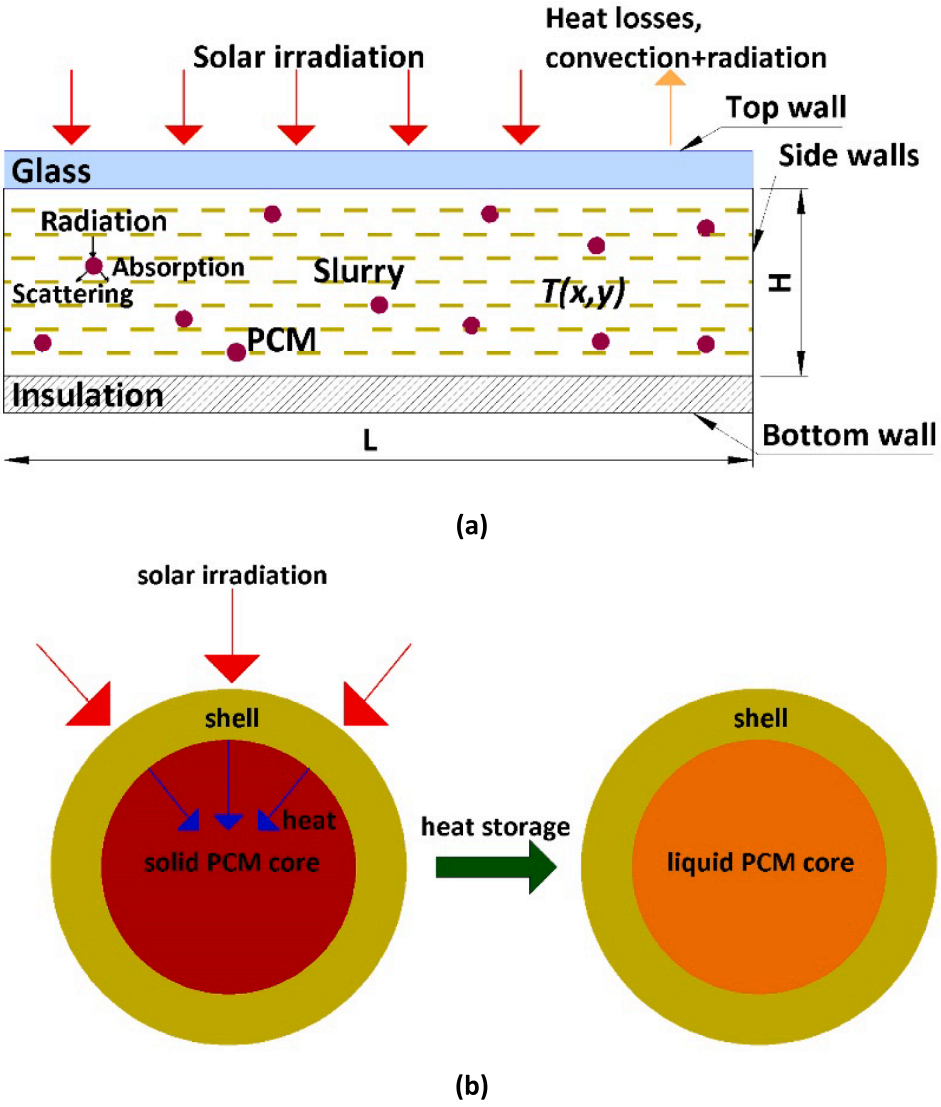

Fig. 1. (a) The graphic illustration of PCS-based direct absorption solar collector, (b) encapsulated PCM.

PCMs with low thermal conductivity, however, cannot interact directly with heat transfer fluid due to leakage during phase change [25]. Encapsulation techniques can be applied that can augment the thermal performance of PCMs by encasing them in a shell. By doing so, we could preserve shape of PCM and prevent leaks [25]. Thus, the encapsulated PCM can be easily incorporated into the heat transfer fluid. Latent functional thermal fluids (LFTLs) formed by dispersing encapsulated PCMs in the heat transfer fluid are a type of phase change slurries (PCSs). Since PCSs have higher thermal performance than pure heat transfer fluids, they can be employed as a working fluid to enhance the overall efficiency of solar energy systems [26,27,28]. Yu et al. [29] analysed the microencapsulated phase change material (MPCM) slurry and investigated the thermal performance of a photovoltaic/thermal (PV/T) module by varying fluid velocities, melting temperatures and slurry concentrations. The numerical results exhibited that increasing concentration boosted the energy and exergy efficiencies. It was found that the best electrical and thermal efficiencies were obtained at low melting temperature while a higher liquidus temperature would be chosen for exergy improvement. The highest enhancements in exergy and energy efficiencies were 3.23 % and 8.3 %, respectively. The effect of microencapsulated phase change slurry (MPCS) on electrical and thermal capacities of a photovoltaic thermal solar collector were numerically explored by Liu et al. [30]. Overall, the electrical and thermal efficiencies, fluid's pressure drop and outlet temperature, and solar cell temperature were measured. The results revealed that when MPCS was used, the collector performance (electrical and thermal) was improved since the change in temperature of both fluid and PV cells was less compared to water. The highest net efficiency was obtained at slurry concentration of 10 wt%, piping height of 10 mm and flow rate of 0.02 kg/s. The maximum average exergy efficiency 11.4 % was found during the morning. Furthermore, it was the average efficiency was found to be 80.57 % at 11am.

In direct absorption solar energy systems, since the absorbing environment of solar radiation is employed both as a working fluid and as a storage medium, PCSs can be adapted to the system, improving both collector performance and latent heat storage. Wang et al. [31] performed an experiment and investigated the impact of microencapsulated phase change materials (MPCMs) dispersed in multi-walled carbon nanotube (MWCNT) nanofluid on photothermal conversion efficiency. The results displayed that the temperature gain diminished with the use of MPCM-MWCNT slurry due to the heat absorption and surface reflectance of MPCM. It was seen that the MPCM-MWCNT slurry's terminal temperature with 15 wt% MPCMs was 4.6 °C higher than the ethanol/water mixture. The effect of microencapsulated paraffin/Cu-Cu_2O/CNTs PCM dispersed in water on thermal performance was conducted by Xu et al. [32]. While paraffin was used as core, Cu, carbon

nanotubes (CNTs), and Cu_2O were chosen as shell material. According to the experimental results, this kind of heat transfer fluids enhanced the light absorption, thermal conductivity, photothermal conversion, and specific heat of the total system. Liu et al. [33] experimentally analysed the thermal performance of the paraffin/MF/graphite micro-encapsulated PCC dispersed in ionic liquid, where paraffin and graphite nanoparticles filled melamine–formaldehyde (MF) were used as a core and shell, respectively, as a heat transfer fluid. The outcomes revealed that the PCC increased the fluid's temperature from 30 to 113 °C. It was found that the storage capacity of the pure ionic liquid was half that of the composite based-ionic fluid.

1.1. Contribution of this paper

As stated in the literature review, although there are studies on nanofluid-based DASCs and PCM and PCS based solar energy systems, there are still significant research gaps regarding the thermophysical behaviour and applications of LFTFs in DASC collectors. Therefore, the current study focuses on nanoencapsulation of PCM with inorganic shell materials. Such nanoencapsulated PCM is dispersed in a base fluid (also referred to as PCS) and the utilization of this material as a new working fluid in a DASC is demonstrated. The impacts of thermophysical and optical characteristics of PCS on the photothermal conversion and storage performance of the system are evaluated. Besides, PCM size changes need to be investigated as they alter the thermophysical and optical characteristics of the slurry. Since the PCM mass concentration also impacts the specific heat performance of the heat transfer fluid, it is a matter of curiosity to what extent it influences the system performance.

Furthermore, the effect of nano encapsulated PCM with metallic shell on the phase change process due to mass concentration, size change of the PCM and different shell materials, as well as the radiation heating, needs to be studied to get the best performance augmentation. Moreover, the effect of hybrid slurries formed with nanoparticles dispersed in host fluid based nano encapsulated PCMs needs to study to enhance the energy conversion performance. Last but not the least, it is required to analyse the influence of thermal radiation coupled with natural convection on volumetrically heated LFTFs since when this combined effect penetrates the nano-size paraffin with metallic shell nano-capsules, its impression on the thermal performance of the collector is unknown. When these are evaluated, the aspiration of the present research is to fill these knowledge gaps regarding the photothermal conversion and storage performance of PCSs in DASC using a comprehensive parametric study and numerical simulations.

2. Modelling and methodology

Fig. 1(a) represents that sunlight penetrates a 2D DASC of length L and height H vertically. The collector is filled with PCS which is heated by irradiation thanks to the highly transparent glass surface. Since it is utilized for storage applications, the bottom and side walls are adiabatic while the heat loss occurs through the glass wall towards the ambient by a combined radiation and convection. Furthermore, as shown in Fig. 1 (b), the encapsulated PCM comprises two parts; the shell and the solid core PCM. As the temperature of the solid PCM approaches its melting temperature, the PCM begins to melt and transforms into liquid PCM. However, the shell that encases the PCM prevents leakage during the phase transformation, preventing its mixing with the base fluid. An aspect ratio (L/H) of 10 is selected as suggested elsewhere [13].

The Radiative Transport Equation (RTE) is employed to determine the radiation's spectral inside the translucent medium, and can be indicated as [34]:

$$\nabla \bullet (I_\lambda(\vec{r},\vec{s})\vec{s}) + (\alpha_\lambda+\sigma_s)I_\lambda(\vec{r},\vec{s}) = \alpha_\lambda n^2 I_{b\lambda} + \frac{\sigma_s}{4\pi}\int_0^{4\pi} I_\lambda(\vec{r},\vec{s}')\Phi(\vec{s}\bullet\vec{s}')d\Omega' \quad (1)$$

The base fluids' scattering effects can be disregarded due to the domination of absorption into the attenuation, thus the extinction coefficient of pure fluids is given as [35]:

$$K_{e\lambda,bf} = K_{a\lambda,bf} = \frac{4\pi k}{\lambda} \quad (2)$$

The absorption and scattering efficiencies for core–shell structures can be obtained with the dipole model [36,37]:

$$Q_{sca} = C_{sca}/(\pi a^2) = \frac{k^4}{6\pi}|\alpha|^2/(\pi a^2) = \frac{128\pi^5}{3\lambda^4}\varepsilon_3^2 r_2^6\left|\frac{\varepsilon_2\varepsilon_\alpha-\varepsilon_3\varepsilon_b}{\varepsilon_2\varepsilon_\alpha+2\varepsilon_3\varepsilon_b}\right|^2/(\pi a^2) \quad (3)$$

$$Q_{abs} = C_{abs}/(\pi a^2) = kIm(\alpha)/(\pi a^2) = \frac{8\pi^2\sqrt{\epsilon_3}}{\lambda}r_2^3 Im\left(\frac{\varepsilon_2\varepsilon_\alpha-\varepsilon_3\varepsilon_b}{\varepsilon_2\varepsilon_\alpha+2\varepsilon_3\varepsilon_b}\right)\Big/(\pi a^2) \quad (4)$$

where C_{sca} and C_{abs} scattering and absorption cross sections, respectively. $k = 2\pi n/\lambda$ and α is the polarizability, and given as [38]:

$$\alpha = 4\pi r_2^3[(\varepsilon_2\varepsilon_\alpha-\varepsilon_3\varepsilon_b)/(\varepsilon_2\varepsilon_\alpha+2\varepsilon_3\varepsilon_b)] \quad (5)$$

where ε_α and ε_b are the effective dielectric functions, and are given as [38]:

$$\varepsilon_\alpha = \varepsilon_1(3-2P)+2\varepsilon_2 P \quad (6)$$

$$\varepsilon_b = \varepsilon_1 P + \varepsilon_2(3-P) \quad (7)$$

$$P = 1-(r_1/r_2)^3 \quad (8)$$

where ε_1, ε_2 and ε_3 are dielectric functions of core, shell, and outer region, respectively. r_1 and r_2 are radii of core and shell, respectively, and P is the ratio of shell volume to total volume of core–shell particle.

The extinction coefficient of the core–shell structure is given by [39]:

$$K_{e\lambda} = C_{ext}N_T = \left(\pi a^2(Q_{abs}+Q_{sca})\right)\left(6n/\pi D^3\right) \quad (9)$$

where n is the concentration of the shell.

As a result, the fluid's total extinction coefficient can be written as the sum of both the particles and the base fluid:

$$K_{total,e\lambda} = K_{f,e\lambda} + K_{e\lambda} \quad (10)$$

The scattering and absorption coefficients of the core–shell structures, however, depend on the dielectric function of the metallic shells. Since the metallic particles' dielectric function is size dependent, it can differ from the bulk material. Therefore, dielectric functions are calculated using the modified Drude model to show the effect of size-dependent optical properties of the metallic shell [38].

$$\varepsilon(w) = \varepsilon_{bulk}(w) + \frac{w_p^2}{w^2+iw\gamma_\infty} - \frac{w_p^2}{w^2+iw\gamma(R)} \quad (11)$$

where w_p is bulk plasma frequency, ε_{bulk} is the dielectric function of the metallic shell, γ_∞ is inverse of the bulk relaxation time [37], $\gamma(R)$ is the scattering rate [37], and R is the effective average free path [40].

$$R = \frac{1}{2}\left[(r_{shell}-r_{core})\left(r_{shell}^2-r_{core}^2\right)\right]^{1/3} \quad (12)$$

$$\gamma_\infty = \frac{1}{\tau_{bulk}} = \frac{1}{l_\infty/V_f} \quad (13)$$

$$\gamma(R) = \frac{1}{l_\infty/V_f} + \frac{AV_f}{R} \quad (14)$$

where l_∞ is the bulk free electron mean free path, V_f is the Fermi velocity, A is the geometric parameter as [37], and τ_{bulk} is the metal free

Table 1
Fermi velocity, bulk plasma frequency, and bulk mean free path of materials [45].

	Ag	Al	Au	Cu
Bulk mean free path (nm)	52	16	42	42
Fermi velocity (10^6 m/s)	1.39	2.03	1.38	1.57
Bulk plasma frequency (10^{16} Hz)	1.36	2.4	1.37	1.64

Table 2
Thermophysical properties of the core and shell materials [50,51,52,53,54].

	ρ (kg/m^3)	k (W/mK)	C_p (J/kgK)	H (J/kg)
n-Octadecane (solid)	814	0.35	2140	245,000
n-Octadecane (liquid)	775	0.149	2660	
Al	2700	247	900	
Ag	10,500	429	235	
Au	19,320	314.4	128.8	
Cu	8954	400	383	

electron scattering time. The Fermi velocity, bulk plasma frequency, and bulk mean free path for each material are given in Table 1. The optical properties of the shell, core and base materials can be found elsewhere [41,42,43,44].

The PCS is supposed to be Newtonian, incompressible, single phase, and laminar. The governing and energy equations are indicated as:

Continuity equation:

$$\frac{\partial u}{\partial x}+\frac{\partial v}{\partial y}=0 \tag{15}$$

x-momentum equation:

$$u\frac{\partial u}{\partial x}+v\frac{\partial u}{\partial y}=-\frac{1}{\rho_{PCS}}\frac{\partial p}{\partial x}+\frac{\mu_{PCS}}{\rho_{PCS}}\left(\frac{\partial^2 u}{\partial x^2}+\frac{\partial^2 u}{\partial y^2}\right) \tag{16}$$

y-momentum equation:

$$u\frac{\partial v}{\partial x}+v\frac{\partial v}{\partial y}=-\frac{1}{\rho_{PCS}}\frac{\partial p}{\partial y}+\frac{\mu_{PCS}}{\rho_{PCS}}\left(\frac{\partial^2 v}{\partial x^2}+\frac{\partial^2 v}{\partial y^2}\right)+\frac{(\rho\beta)_{PCS}}{\rho_{PCS}}g(T-T_0) \tag{17}$$

Conservation of energy:

$$\rho_{PCS}C_{p\,PCS}\left(u\frac{\partial T}{\partial x}+v\frac{\partial T}{\partial y}\right)=k_{PCS}\left(\frac{\partial^2 T}{\partial x^2}+\frac{\partial^2 T}{\partial y^2}\right)-\nabla\bullet q_r \tag{18}$$

The boundary conditions are represented as:
at all solid walls:

$$u=v=0 \tag{19}$$

at the upper wall:

$$q=h(T-T_{amb})+\varepsilon\sigma(T^4-T_{amb}^4) \tag{20}$$

at the bottom wall:

$$\frac{\partial T}{\partial y}=0 \tag{21}$$

at the side walls:

$$\frac{\partial T}{\partial x}=0 \tag{22}$$

The convective heat transfer coefficient, h, is calculated by Duffie correlation [46]:

$$h=5.7+3.8v \tag{23}$$

The density of PCS, ρ_b, is calculated as [47]:

$$\rho_b=\frac{\rho_p\rho_f}{\rho_f c_m+\rho_p(1-c_m)} \tag{24}$$

where the subscripts f, p, and b denote the base fluid, particle, and slurry. c_m is the mass concentration. The density of encapsulated PCM, ρ_p, is calculated as [47]:

$$\rho_p=\frac{(1+y)\rho_c\rho_s}{\rho_s+y\rho_c} \tag{25}$$

where the subscripts c and s denote the core and shell, respectively. y is the core–shell weight ratio, and it is calculated as [47]:

$$\left(\frac{d_c}{d_p}\right)^3=\frac{\rho_s}{\rho_s+y\rho_c} \tag{26}$$

where d is the diameter.

The thermal conductivity of the PCS, k_b, is calculated as [47]:

$$k_b=k_f\frac{k_p+2k_f+2(k_p-k_f)c_v}{k_p+2k_f-(k_p-k_f)c_v} \tag{27}$$

where k_p and c_v are the thermal conductivity encapsulated PCM and volume concentration, respectively. They are calculated as [47]:

$$\frac{1}{k_p d_p}=\frac{1}{k_c d_c}+\frac{d_p-d_c}{k_s d_p d_c} \tag{28}$$

$$c_v=\frac{c_m\rho_b}{\rho_p} \tag{29}$$

The specific heat of the PCS, $C_{p,b}$, depends on the phase change process. The general expression of the specific heat can be calculated as [47]:

$$C_{p,b}=(1-c_m)C_{p,f}+c_m C_{p,p} \tag{30}$$

where $C_{p,p}$ is the specific heat of encapsulated PCM. If there is no phase change process, it is determined as [47]:

$$C_{p,po}=\frac{(C_{p,c}+yC_{p,s})\rho_c\rho_s}{(y\rho_c+\rho_s)\rho_p} \tag{31}$$

When the phase transition occurs, however, the specific heat of encapsulated PCM can be defined as:

$$C_{p,pm}=\frac{H}{T_2-T_1} \tag{32}$$

where H, T_1 and T_2 are the latent heat of PCM, solidus and liquidus temperatures, respectively.

Then the equivalent specific heat capacity of the PCS is expressed as:

$$C_{p,b}=(1-c_m)C_{p,f}+c_m C_{p,po};T<T_1,T>T_2$$

$$C_{p,b}=(1-c_m)C_{p,f}+c_m C_{p,pm};T_1<T<T_2 \tag{33}$$

The viscosity of the PCS, μ_b, is defines as [48]:

$$\mu_b=\left(1-c_v-1.16c_v^2\right)^{-2.5}\mu_f \tag{34}$$

The thermal volume expansion of the PCS, β_b, can be written as [49]:

$$\beta_b=(1-c_v)\beta_f+c_v\beta_c \tag{35}$$

Table 2 also exhibits the thermophysical properties of the materials.

Besides, the numerical modelling for pure nanofluids is found in the published works of authors [55,56].

The stored energy of the thermal system can also be determined as [57]:

$$q_s=\Delta H \tag{36}$$

where ΔH is the enthalpy change and based on the results of the numerical simulations/ANSYS Fluent.

Finally, the thermal enhancement of the DASC between the cases of the PCS and base fluid is described as:

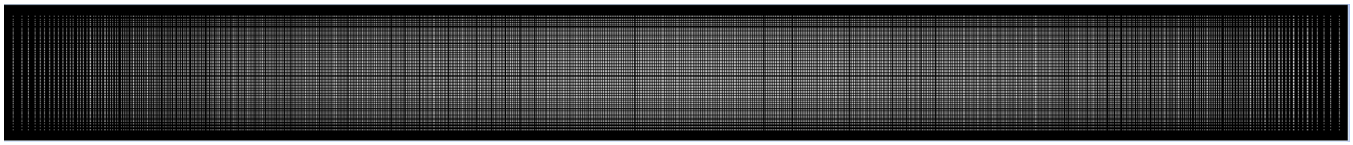

Fig. 2. 2D mesh structure.

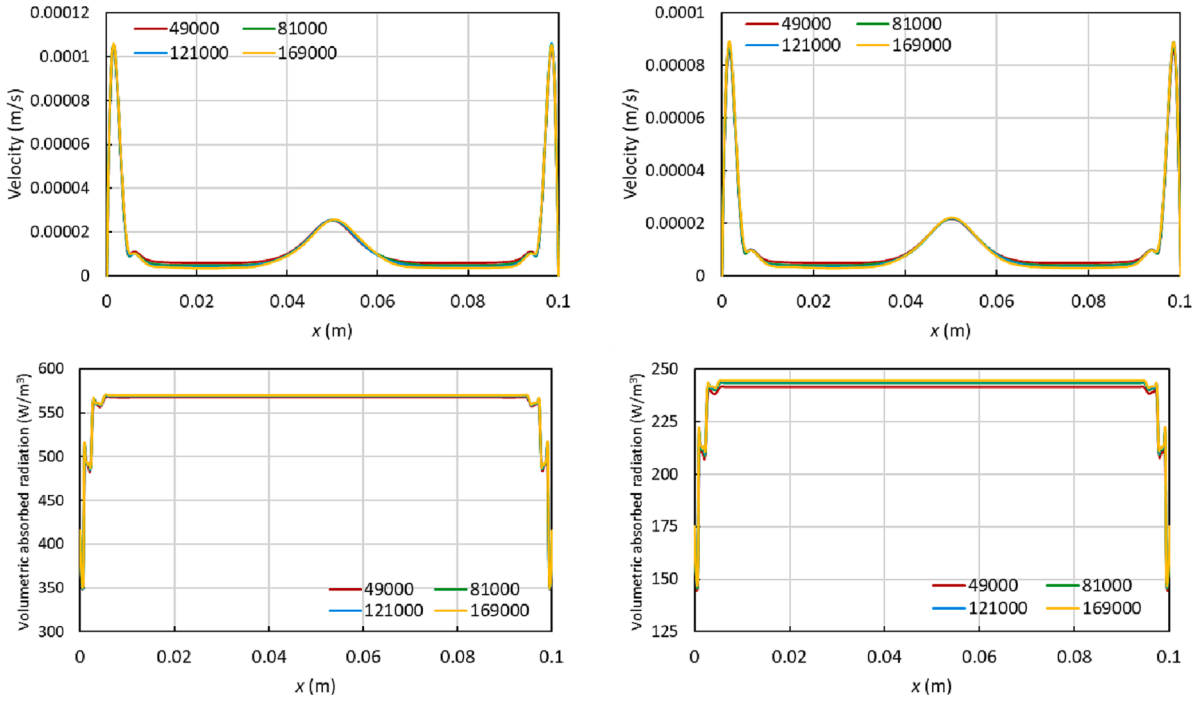

Fig. 3. Variation in velocity and volumetrically absorbed radiation for PCS (left column) and hybrid PCS (right column) with different mesh densities.

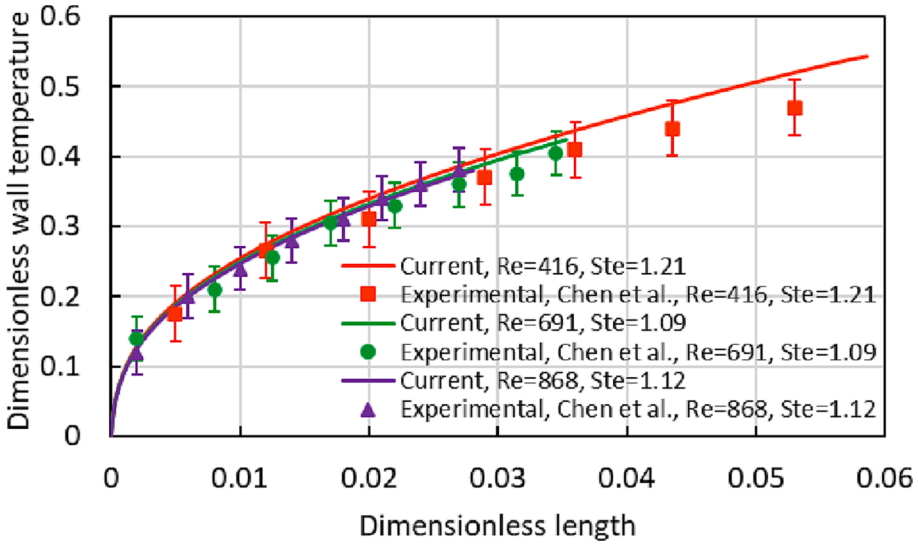

Fig. 4. Comparisons between current and experimental results [47].

$$E = \frac{(thermal\ \ variable)_{PCS} - (thermal\ \ variable)_{host\ \ fluid}}{(thermal\ \ variable)_{host\ \ fluid}} \tag{37}$$

where the thermal variable demonstrates here either the temperature gain as the temperature change between the final and initial temperatures of the PCS or energy storage.

3. Computational model

The governing equations are solved using ANSYS Fluent 2020 R1 which is based on the FVM. The Discrete Ordinates (DO) method is chosen to resolve the RTE that contains influences of absorbing, scattering, and emitting factors. The SIMPLE algorithm is utilized for the

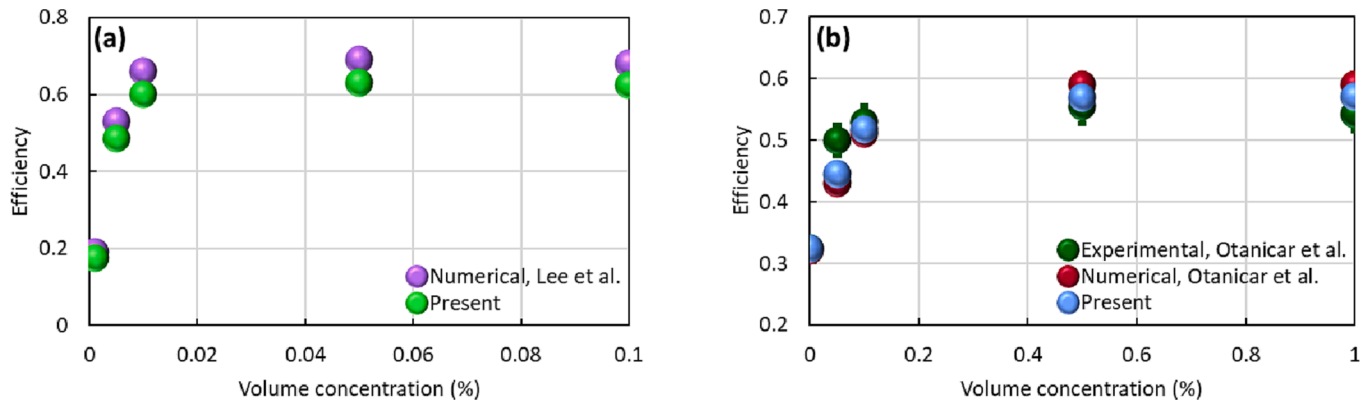

Fig. 5. Comparison of the collector efficiency with benchmark results [58,59].

Table 3
Comparison of findings for mean Nusselt number with literature.

	Present	Khanafer et al. [50]
$Gr = 10^3$	2.1	2.2
$Gr = 10^4$	4.3	4.4
$Gr = 10^5$	8.6	9.1

velocity–pressure coupling. The second-order upwind differencing scheme is employed to discretize the equations so as to get more acceptable results. PRESTO! and Least Squares Cell Based are made use of for pressure and gradient, respectively. The convergence values are set below 10^{-5} for the continuity and momentum equations and below 10^{-6} DO and energy equations to achieve better results. 3X3 Pixels and 5x5 Divisions are chosen to achieve more precise results [34]. Moreover, the detailed information for the resolution of governing and energy equations is found in the previous studies of Kazaz et al [55,56].

3.1. Mesh dependency test

A grid sensitivity examination is performed before performing the simulations to confirm that the results are independent of the mesh density. The non-uniform mesh within the computational domain is created, and the 2D schematic representation of the mesh structure is demonstrated in Fig. 2. The grid refinement results are compared. As illustrated Fig. 3, the mesh numbers of 49000, 81000, 121000 and 169000 are chosen for both fluid types: PCS and nanoparticle-based PCS, and the temperature and volumetric absorbed radiation are compared for the grid refinement results. The mesh numbers of 81000, therefore, is chosen for the further simulations to get more accurate and reliable results and reduce the computational time.

3.2. Model validation

The experimental results reported by Chen et al. [47] were utilized to validate the equivalent specific heat capacity predicted in this study for

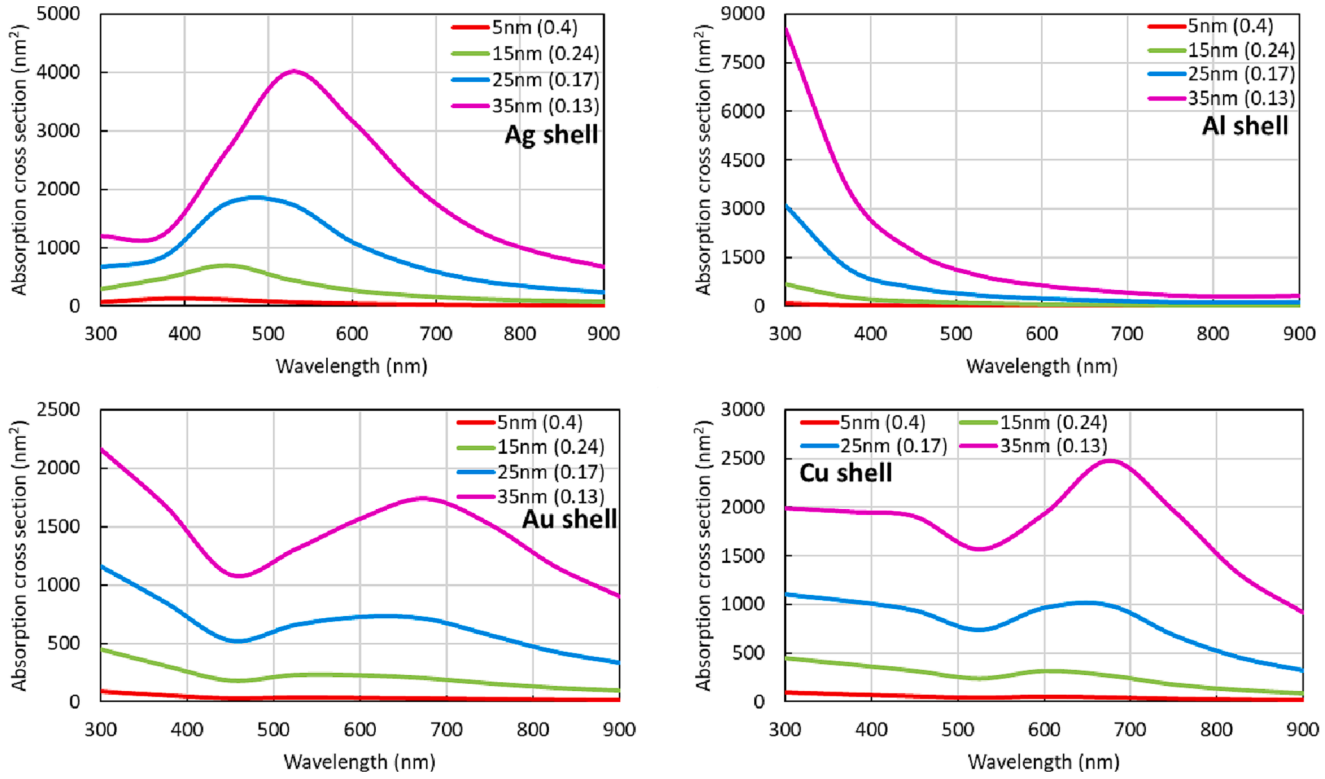

Fig. 6. Effect of core size (surface-to-volume ratio of the nano capsule, m^{-1}) on absorption cross section with different shell materials.

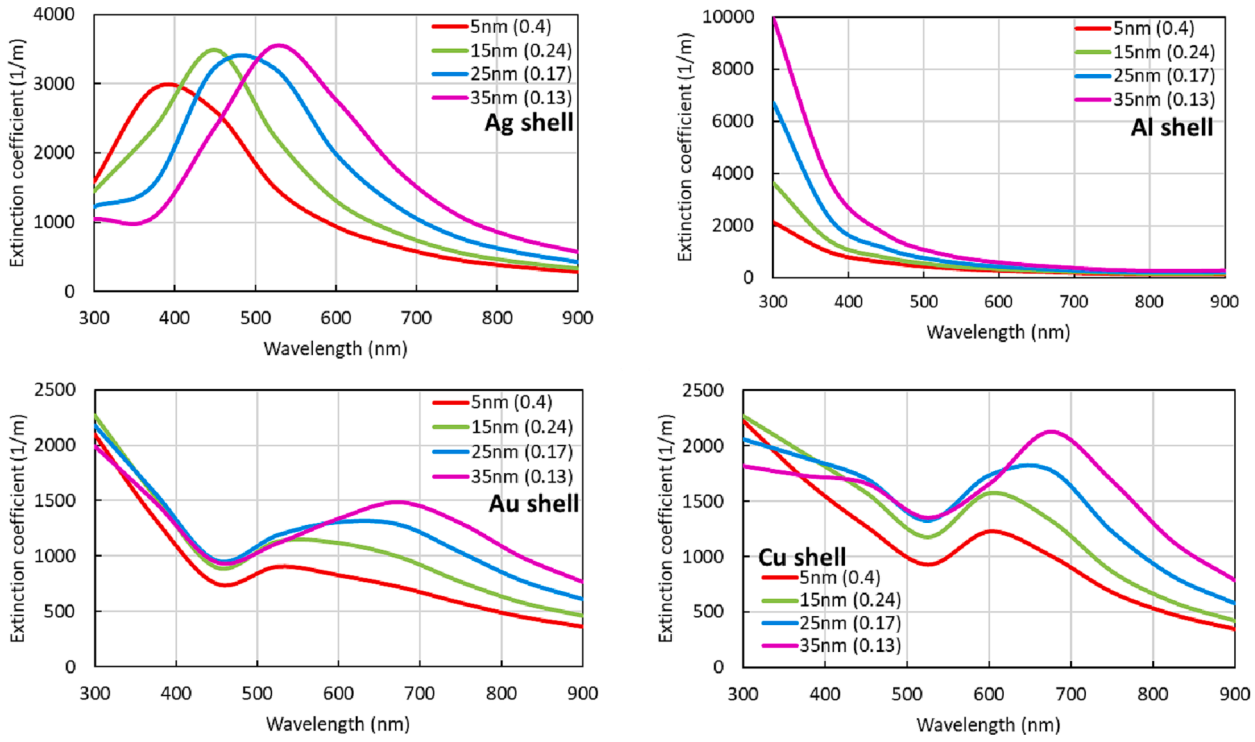

Fig. 7. Effect of core size (surface-to-volume ratio of the nano capsule, m^{-1}) on extinction coefficient with different shell materials.

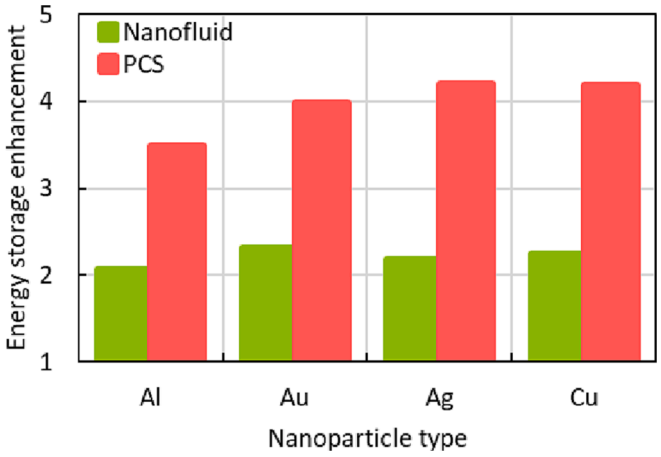

Fig. 8. Comparative thermal performance analysis of nanofluid and PCS.

the first validation case. The experimental study considered a circular tube of 4 mm diameter and 1.46 m length. The microparticles comprised Amino Plastics (Urea-formaldehyde) shell and industrial-grade 1-bromo-hexadecane ($C_{16}H_{33}Br$) core and water was selected for the host fluid. Dimensionless wall temperature $\left(\theta_{w,x} = \left(T_{w,x} - T_{b,i}\right)/\left(\ddot{q_w}r/k_b\right)\right)$ and dimensionless axial length $\left(x^+ = (x/r)/(Re_bPr_{bo})\right)$ were used to analyse the results. Fig. 4 compares the dimensionless wall temperature with dimensionless length for Stefan number 1.21, 1.09, and 1.12 using a microencapsulated phase change material mass concentration of 15.8 %.

The study of Lee et al. [58], which performs numerical investigation to verify the radiation/optical model, was chosen for the second validation. The SiO_2/Au core/shell capsules as non-metallic and metallic materials, respectively dispersed in pure water enters the DASC in which the heat loss coefficient of 6 $Wm^{-2}K^{-1}$ takes place from glass wall to the atmosphere. The glass wall is also exposed to solar irradiation density of 1367 W/m^2. The working fluid's inlet temperature is 293.15 K. The comparative results between current and benchmark cases for collector efficiency is displayed in Fig. 5(a) as the maximum error of 9.1 %. Further, the current results are compared with the experimental results of Otanicar et al. [59] for the radiation model. The Graphite/water working fluid with a flow rate of 0.7 ml/minute enters the DASC in which the heat loss of 23 $Wm^{-2}K^{-1}$ takes place from glass wall to the atmosphere by a combined convection and radiation. The comparative results between current and benchmark [59] cases for collector efficiency are displayed in Fig. 5(b) as the maximum error of 11 %.

The fourth validation study compares results with those of Khanafer et al. [50] to examine the investigate of free convection in a square closed cavity. The cavity is filled with Cu/water nanofluid with a particle fraction of 5 %. The bottom and top plates of the enclosure are adiabatic whereas side walls are kept at constant cold and hot temperatures. The average convective Nusselt numbers on the hot wall prediction is summarised in Table 3. As distinguished in validation studies, the current findings match well with the benchmark cases as the maximum and mean errors of 5.49 % and 4.03 %, respectively.

4. Results and discussion

This part first emphasizes the optical properties of the core/shell structure, then compares the performance of nanofluids and phase change slurry and highlights the effects of nano capsule size, different shell material types, mass concentration of PCM, and hybrid phase change slurry on photothermal conversion and storage. The size of the core and core/shell structure is also compatible with other studies such as [39,60,61,62].

4.1. Optical properties

The core/shell structure consisting of paraffin (PCM) core and silver (Ag), aluminium (Al), copper (Cu), and gold (Au) shells. Since both the core and shell materials have different optical properties, the optical characteristics of the core–shell constructions formed by different types

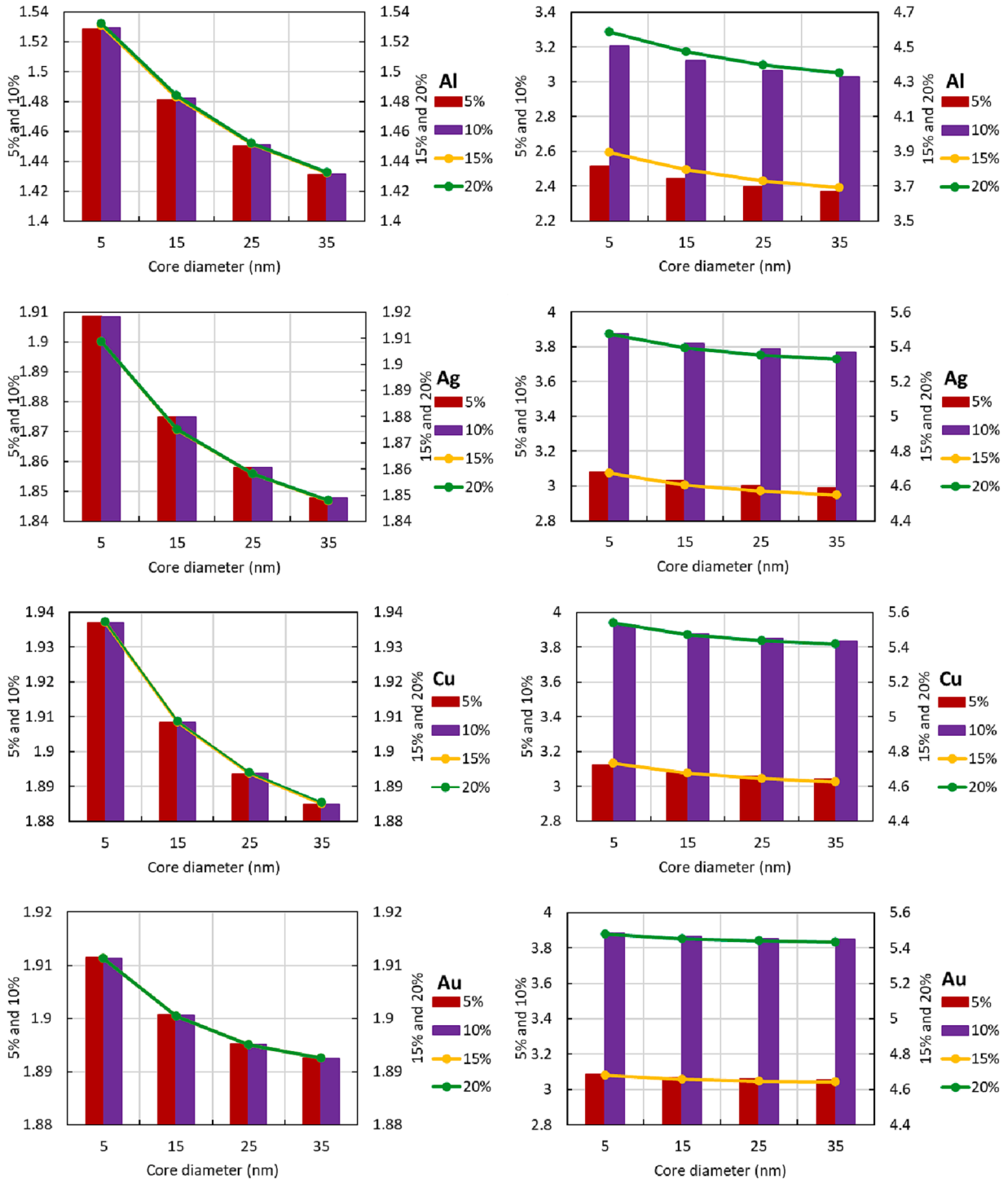

Fig. 9. Effect of shell material and PCM mass concentration on temperature gain (left column) and stored energy (right column) enhancements.

of shell materials with paraffin also differ.

The impacts of shell material and core size on optical properties are demonstrated in Fig. 6. The diameter of the PCM (or surface area-to-volume ratio of the nano capsule) are considered as 5 nm (0.4 m^{-1}), 15 nm (0.24 m^{-1}), 25 nm (0.17 m^{-1}) and 35 nm (0.13 m^{-1}). The differences in the effects of increasing core size and changing shell materials on both the scattering and absorption cross sections between the wavelengths can be explained as the surface plasmon resonance effect as seen in Fig. 6. Since the materials used as the shell structure are metallic, they have free electrons in their surface layers. This surface layer, which is exposed to sunlight, creates the vibration frequency between radiation and electrons, stimulating the surface plasmon resonance and providing the formation of absorption peak positions. As shown in Fig. 6, the absorption peaks are seen in a certain way, especially in the absorption section. Enhancing core size causes the surface area-to-volume ratio decrease, the peaks become more pronounced, and the core diameter is 35 nm, that is, if the surface area-to-volume ratio of PCM is minimum as 0.13 m^{-1}, it takes the maximum value. This finding is consisted with that of Wu et al. [39] who explored that it is augmented with enhancing total size. While the maximum peak in paraffin/Ag core/shell structure occurred at 525 nm wavelength, it occurred at 675 nm wavelength in paraffin/Au and paraffin/Cu structures. However, a more uniform

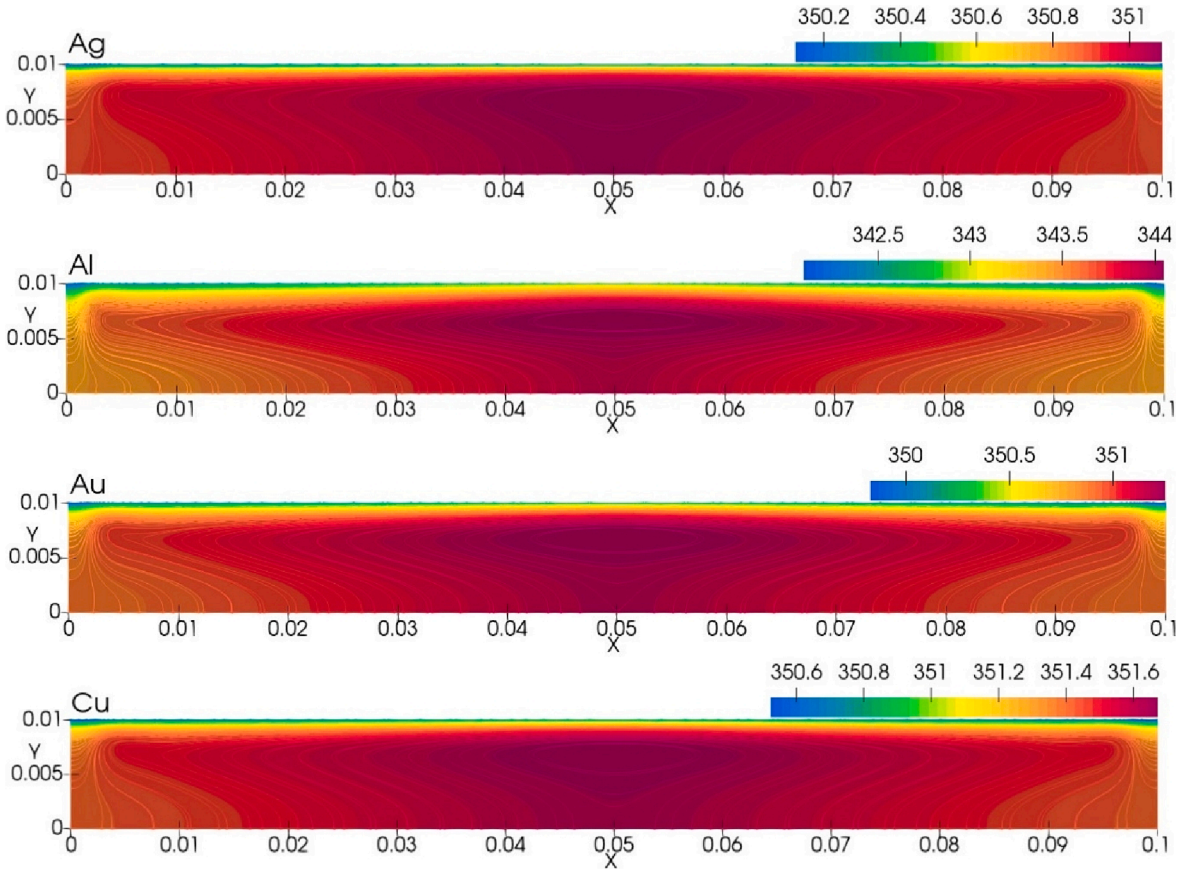

Fig. 10. Temperature (K) contours at core diameter of 5 nm and PCM mass concentration of 5 %.

absorption curve in the paraffin/Al core/shell structure is observed at 300 nm wavelength compared to other structures. The reason for this can be understood from Table 1. It is seen that the Al material has the highest bulk plasma frequency. Besides, when the surface area/volume ratio of PCM is 0.4 m^{-1} and 0.24 m^{-1}, it is seen that the peaks are less prominent.

The effect of paraffin-based core/shell structure with varying core diameter of different shell materials on the extinction/attenuation coefficient is demonstrated in Fig. 7. The surface plasmon resonance, which is activated due to the interaction of the electrons in the metal shells with the irradiation, creates the absorption peak positions and shifted these peak waves to larger wavelengths with the increase of the core diameter. As seen in Fig. 7, enhancing the paraffin size from 5 nm to 25 nm in Ag shell material causes a decrease in the surface area-to-volume ratio of the PCM from 0.4 m^{-1} to 0.17 m^{-1}, shifting the peak position of the paraffin/Ag core/shell structure from 400 nm wavelength to 525 nm wavelength. This finding that shifts with enhancing the total size is also declared by Lv. Et al. [37] and Wu et al. [39]. Although the trend in the extinction coefficient of Au and Cu-shelled paraffin structures seems to be the same, it is discovered that the peak positions in the trend paraffin/Cu structure are more prominent. In the paraffin/Al core/shell structure, the extinction coefficient decreases with increasing wavelength, while the diminish in the surface area-to-volume ratio improves the extinction coefficient. However, it is noticed that the attenuation coefficient of the paraffin/Ag core/shell structure increases up to the wavelength at which the peak of the plasma resonance is maximum, while it starts to decrease after it becomes maximum. Further, the rise in the mean attenuation coefficient with the improvement of the capsule size is supported by the study of Wu et al [39] as illustrated in Fig. 7. Finally, the attenuation coefficient is equal to the mean coefficient between these wavelengths [63].

4.2. Comparison of nanofluid and phase change slurry

Comparative analysis of the system in which nanofluid and phase change slurry (PCS) are used as heat transfer fluids is done. Nanofluids are obtained with Al, Au, Ag and Cu nanoparticles dispersed in water. In order to get encapsulated PCM, these nanoparticles are also added to the paraffin core as a shell, forming a core/shell construction and dispersed in water, and thus the PCS is obtained. As indicated in Fig. 8, the energy storage improvements of water-based Al, Au, Ag and Cu nanofluids are 2.06, 2.3, 2.18 and 2.25, respectively. However, paraffin core/shell structure with Al, Au, Ag and Cu shell adds to water, the improvement in stored energy increases by 68.9, 73, 92.66 and 86.2 %, respectively. The reason for such an increase in improvement is the high latent heat capacity of paraffin, that is a PCM. In this way, the PCS significantly enhances the thermal energy storage according to the nanofluid.

4.3. Effect of shell material type on phase change slurry

Core size and shell material type alter the optical characteristics of the capsule. The PCM concentration is another factor affecting the core/shell structure. Therefore, the points affecting the thermal performance of PCS can be considered as core size, shell material type and mass concentration of PCM. The influences of changing core size of PCM with mass concentrations of 5, 10, 15 and 20 % on PCS are investigated by using Al, Ag, Au, and Cu shell materials. Since higher concentrations increase the viscosity of the fluid, leading to non-Newtonian behaviour, the maximum mass concentration is chosen as 20 % [64].

As indicated in Fig. 7, the extinction coefficient of encapsulated PCMs depends on the metallic shell material. Although the extinction coefficient of the paraffin/Al capsule is higher at core diameter of 35 nm than the other structures, it has the lowest effect on both temperature

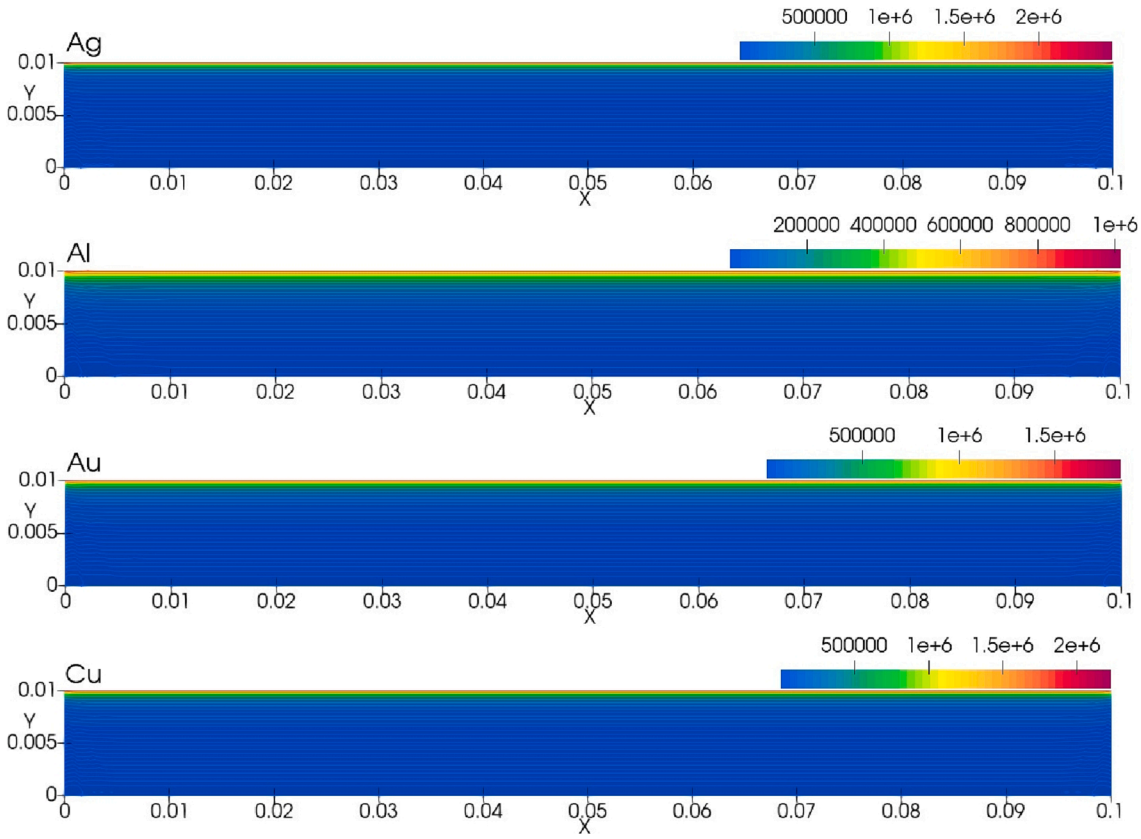

Fig. 11. Volumetric absorbed radiation (Wm^{-3}) contours at core diameter of 5 nm and PCM mass concentration of 5 %.

and energy storage improvement due to the poor thermal conductivity of the Al material, as seen in Fig. 9. Besides, although the changes in the extinction coefficients of paraffin/Cu and paraffin/Au structures are almost similar to each other, since the Cu's thermal conductivity is better than the Au, the enhancements of the paraffin/Cu capsule in temperature and energy storage are relatively stronger by improving photothermal conversion of solar energy. This temperature improvement matches that of Xu *et al.* [32] who compare the thermal behaviour of paraffin-based slurry with pure water.

Furthermore, it is illustrated in Fig. 9 that both the temperature and energy storage augmentation decrease with increasing core size/decreasing surface area-to-volume ratio. Increasing core size also enhances the size of the capsule. The increased amount of total size boosts the volume of the particle at constant concentration, resulting in a decrease in the surface area-to-volume ratio of the core/shell structure. The reduced surface area/volume ratio causes the capsules dispersed in the heat transfer fluid to agglomerate, creating larger particles. By causing an increase in the thermal impediment between these large particles and the working fluid, it reduces the heat that the PCM can take, reducing the temperature of the system and negatively affecting the heat storage. Besides, nano capsules with a high surface area-to-volume ratio have a larger surface area per unit volume to spread. This accelerates the heat transfer between the capsules and allows it to give more heat to the host fluid, and thus it enhances the slurry's temperature. These results reveal those of Ashraf et al. [65] who also discovered that enhancing particle size and agglomeration negatively affect the performance of the nanocomposites.

Moreover, the increase in the mass concentration increasing in the fixed core size provides the augmentation of the stored energy as demonstrated in Fig. 9. But the reason why the improvement in temperature remains constant in the same situation can be explained as the change in the PCM's temperature keeps almost steady in the phase transition process.

As seen in Fig. 10, the heat transfer fluid consisting of core/shell structures absorbs sunlight from the bottom and side walls of the collector and begins to get hotter. Since the collector's side and base walls have high reflectivity, the solar radiation is reflected towards the inside of the solar collector, and the slurry transports up due to the thermal expansion of the PCS, allowing high temperature gradients to form towards the centre of the collector. It is also clearly seen in Fig. 10 that different shell materials affect the thermal performance of the collector differently. Metallic Al material has a 5 nm core diameter, as it is indicated in Fig. 7, its extinction coefficient is lower than other capsules. Besides, since the Al material has the lowest thermal conductivity, both the heat gain (see Fig. 10) and radiation heat generation (see Fig. 11) of the paraffin/Al capsule are the lowest. Furthermore, the thermal performances of paraffin/Ag and paraffin/Cu based slurries in the collector are similar as seen in Fig. 10 and Fig. 11. Since both the thermal conductivities of these two shell materials and the extinction coefficients in the core/shell structures are approximately the same, they show such a tendency. Moreover, as displayed in Fig. 11, the reason for the heat generation by radiation in the collector to decrease with depth is the possibility of collision between the capsules and sunlight, resulting in a decrease in the light intensity and the maximum heat generation occurring around the top plate of the collector.

4.4. *Effect of mono nanoparticle type on phase change slurry*

The most substantial factor affecting the overall photothermal conversion performance of the collector is the heat transfer fluid. The optical and thermophysical characteristics of the working fluid can contribute to the improvement of this performance. As seen in Fig. 9, the slurry consisting of paraffin/Al core/shell structure has the lowest thermal performance when compared with other PCS types. To enhance this capacity, nanoparticles can be added to the slurry where water is the host fluid. These nanoparticles form the hybrid PCS. As the slurry's

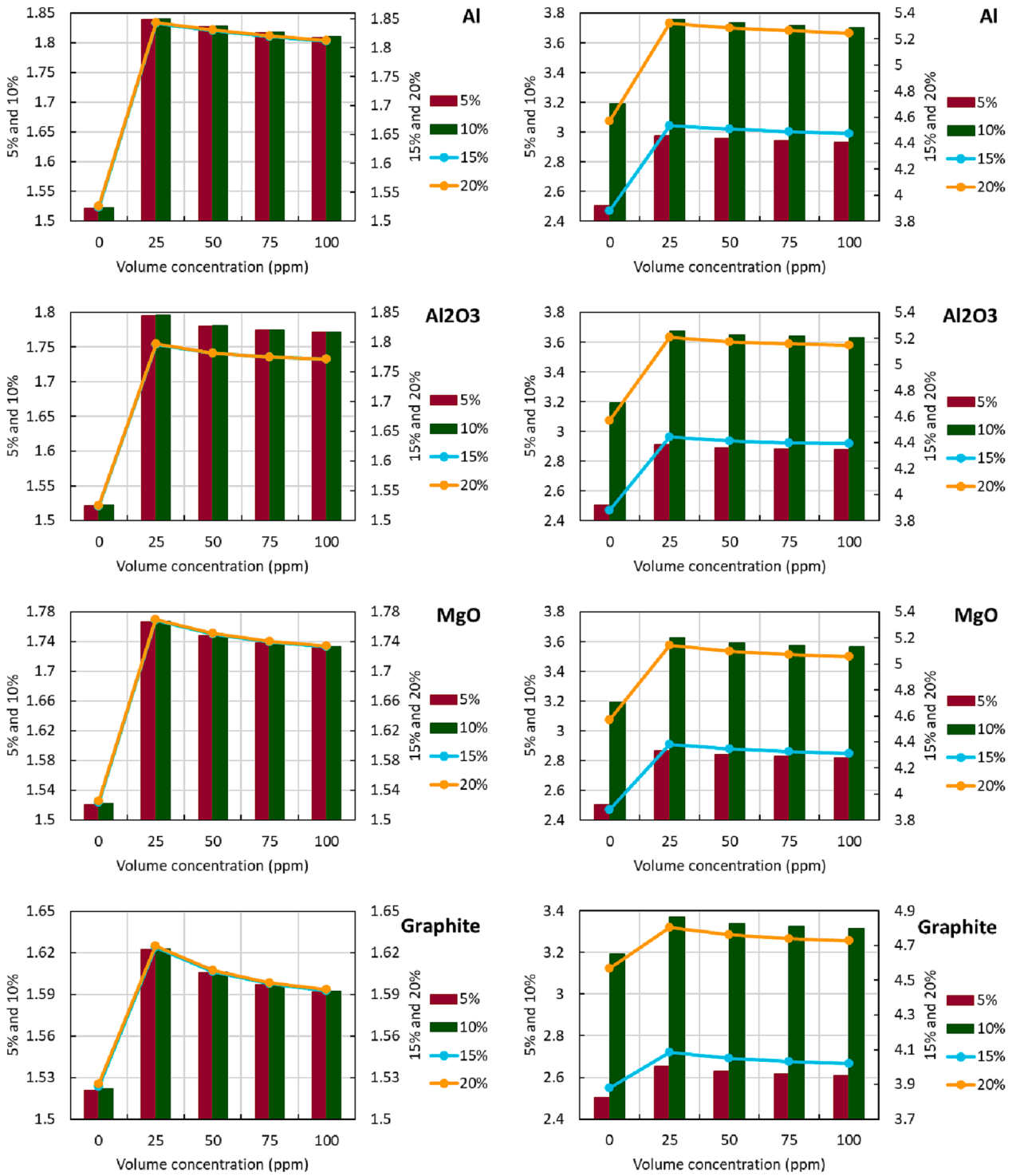

Fig. 12. Effects of addition of mono nanoparticle to PCS and PCM mass concentration on temperature gain (left column) and stored energy (right column) enhancements.

extinction capacity is the sum of the attenuation coefficient of the base fluid, encapsulated PCM, and nanoparticle, it increases the solar energy absorption ability.

As indicated in Fig. 12, Al, Al_2O_3, Graphite and MgO nanoparticles are dispersed to the paraffin/Al based slurry. In the absence of nanoparticles (zero volume concentration), the PCS has the lowest thermal capacity. Since the further nanoparticle addition improves both the optical and thermophysical characteristics of the hybrid PCS, it augments the solar radiation absorbing power of the new working fluid, increasing both the heat gain and the stored energy of the working fluid. This enhancement supports confirmation from earlier examination of Li et al. [66]. In addition, increasing the mass concentration of PCM from 5 % to 20 % in both nanoparticle-free and fixed concentration augments the heat storage by enhancing the enthalpy difference of the slurry more. It is seen that, however, this increase in mass concentration is not too much for temperature gain improvement at constant nanoparticle concentration. It is due to the fact that there is not much change in the temperature of the PCM by absorbing a huge quantity of latent heat

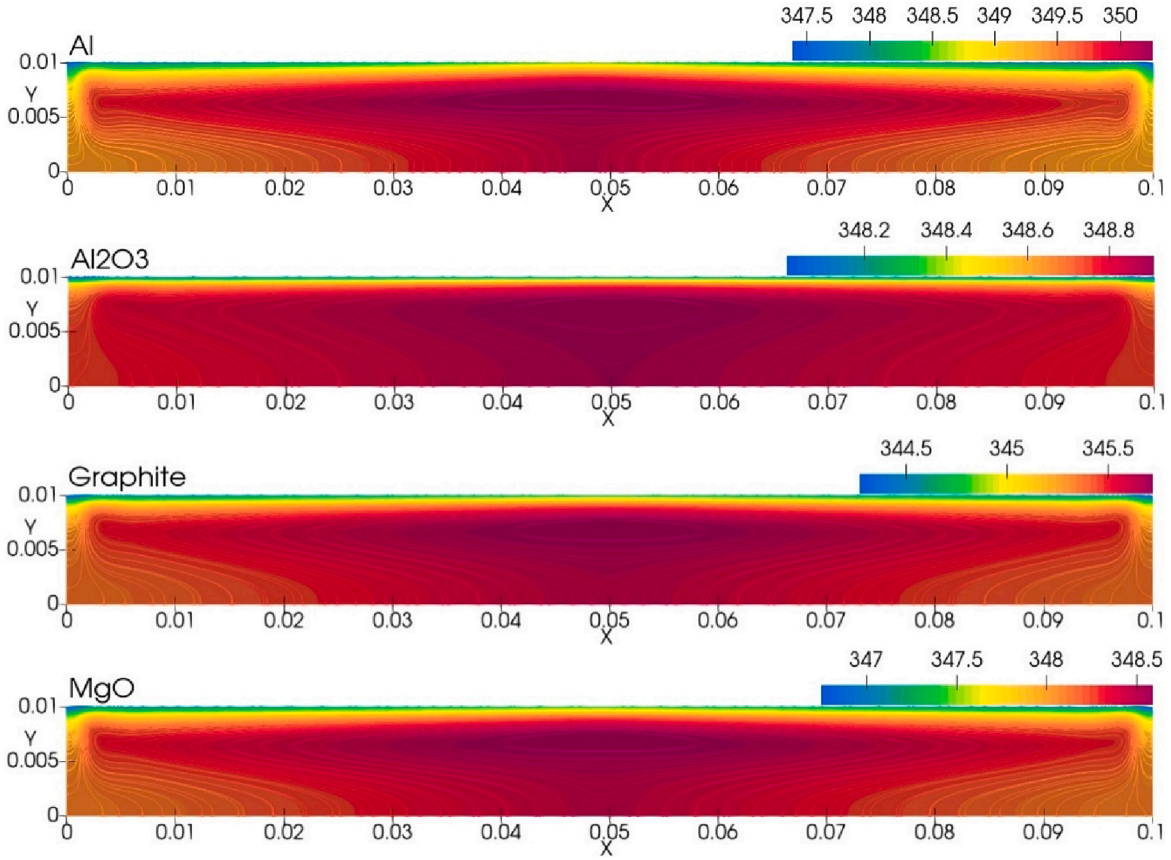

Fig. 13. Temperature (K) contours at volume concentration of 25 ppm and PCM mass concentration of 15 % (Al, Al_2O_3, Graphite and MgO).

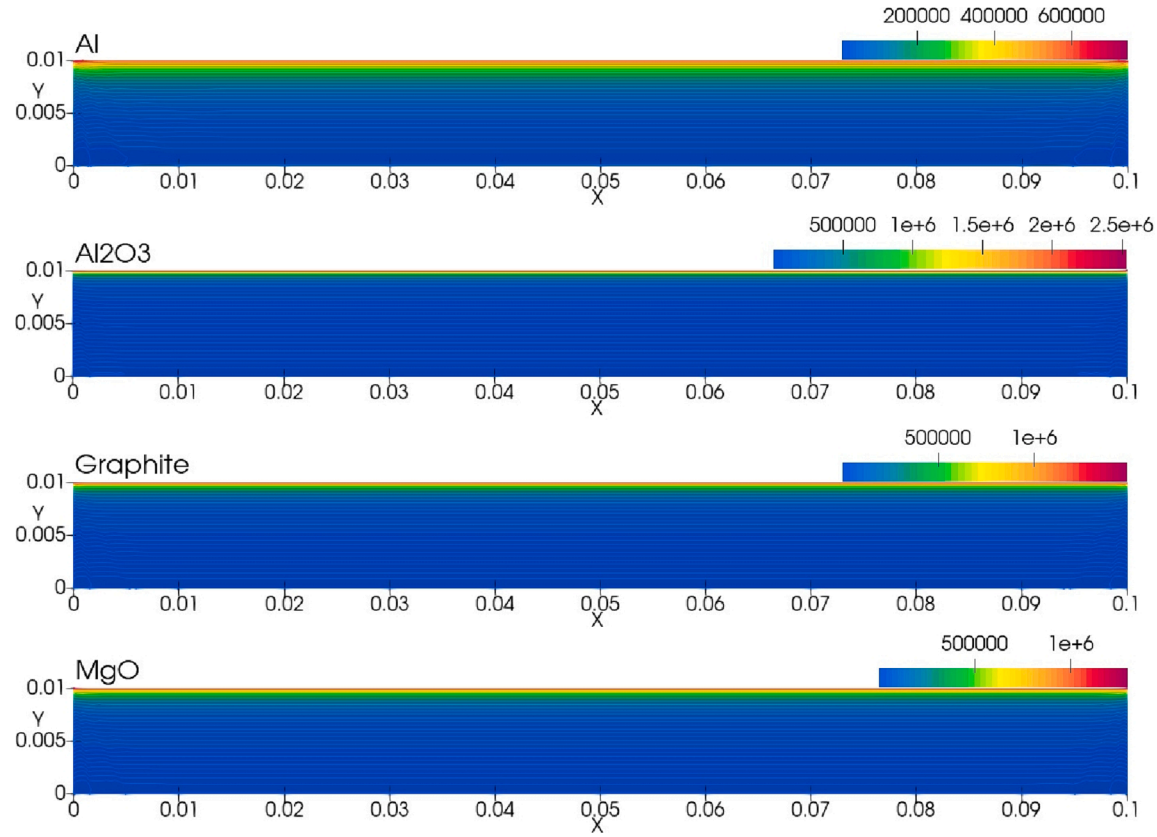

Fig. 14. Volumetric absorbed radiation (Wm^{-3}) contours at volume concentration of 25 ppm and PCM mass concentration of 15 % (Al, Al_2O_3, Graphite and MgO).

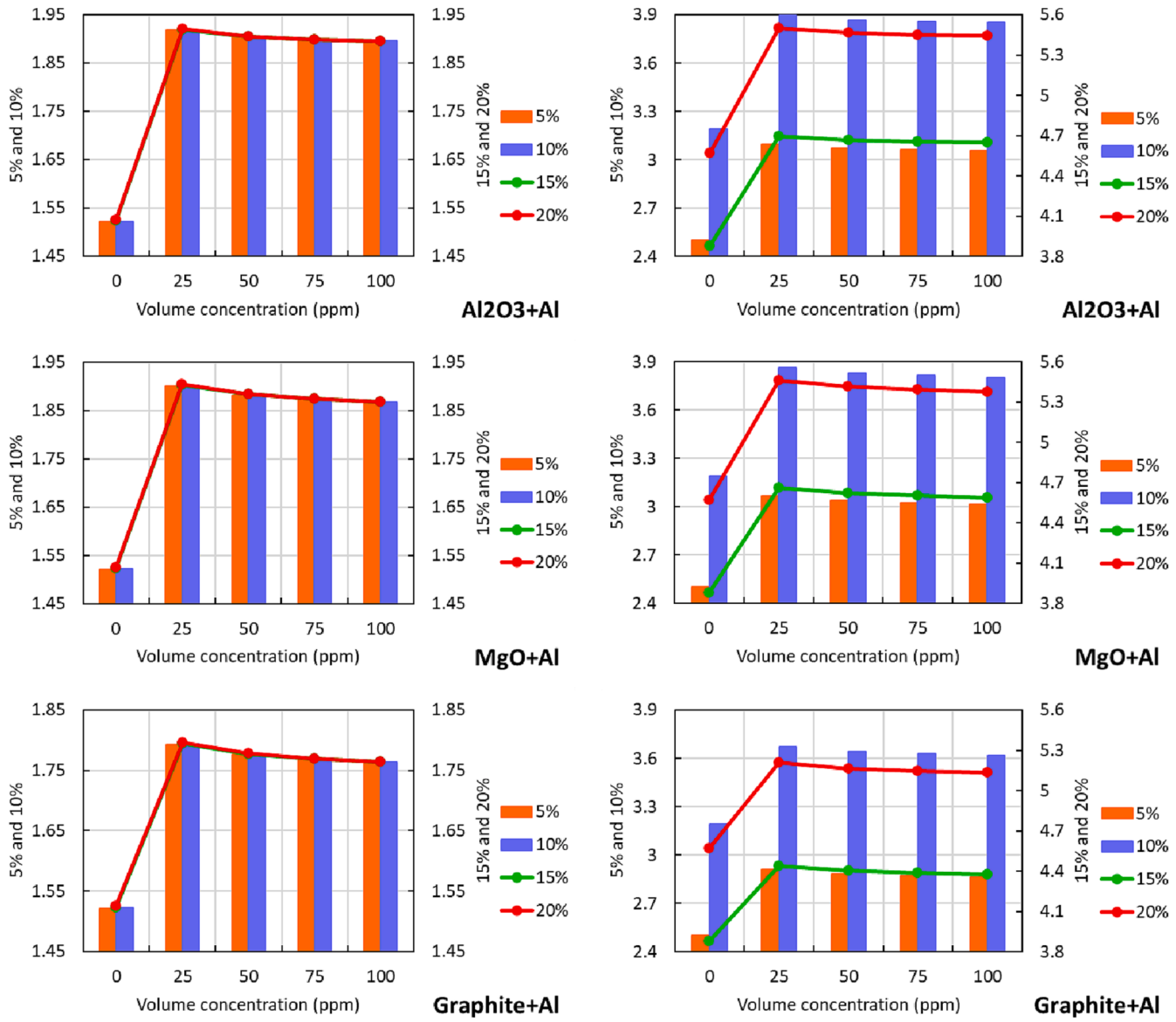

Fig. 15. Effects of addition of hybrid nanoparticle to PCS and PCM mass concentration on temperature gain (left column) and stored energy (right column) enhancements.

during the PCM's phase change transition from solid to liquid state.

It is also seen in Fig. 12 that enhancing nanoparticle concentration slowly decreases both the temperature and storage gain. Improving nanoparticle concentration allows less radiation to penetrate into the collector, reducing heat production. This allows more sunlight to be absorbed by the hybrid PCS around the top plate, reducing both the storage gain and temperature of the fluid.

Furthermore, as signified in Fig. 13, although the nanoparticle addition at constant volume and mass concentration to the slurry makes the temperature gains of the hybrid PCS differ, it is observed that there is not much fluctuation in the maximum temperatures of the slurries. The cause for this can be explained as the phase transition of the PCM by keeping its temperature constant during the phase transition period. Besides, with the penetration of sunlight into the collector, the heating starts from the bottom and side walls, causing the less dense fluid to rise while the denser fluid falls, allowing high temperatures to occur inside the collector. Due to the coupled convection and radiation heat loss from the upper wall of the solar collector to the ambient, the cooling is stronger around the upper wall.

Moreover, the nanoparticle additives increase the working fluid's attenuation coefficient and absorbs more sunlight. It provides an increase in the heat that can be produced from this irradiation in the collector. As revealed in Fig. 14, the average volumetric heat generation is maximum in Al_2O_3 based hybrid PCS, while it is minimum in Al based hybrid PCS. This is because the Al_2O_3 nanoparticles' absorption capacity is stronger compared to other nanoparticles, while that of Al is the lowest. Since the radiation intensity also lessens with the depth, the mean volumetric heat generation decreases towards the bottom of the collector.

4.5. *Effect of hybrid nanoparticle on phase change slurry*

Hybrid nanoparticles can be employed to raise the thermal capacity of the working fluid with low thermal performance. Hybrid nanoparticles dispersed in water will increase the working fluid's ability to capture solar energy more, resulting in greater temperature gain. As demonstrated in Fig. 12, the thermal performance of the water-dispersed Al-based PCS is better than the other fluid types. Therefore, it is a good method to examine the analysis of their thermal performance by creating hybrid nanoparticle-based slurries by adding Al nanoparticles

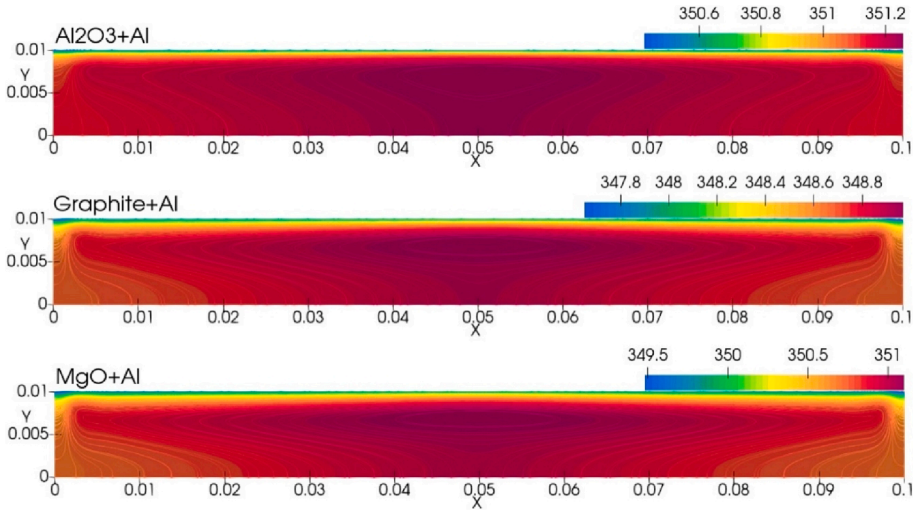

Fig. 16. Temperature (K) contours at volume concentration of 25 ppm and PCM mass concentration of 15 % (Al_2O_3 + Al Graphite + Al and MgO + Al).

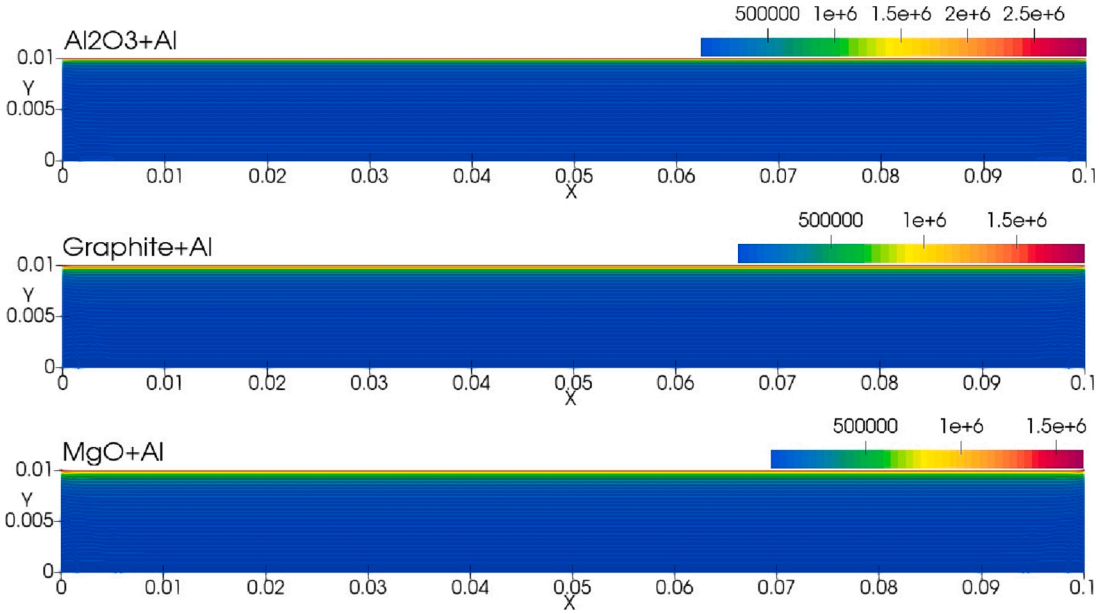

Fig. 17. Volumetric absorbed radiation (Wm^{-3}) contours at volume concentration of 25 ppm and PCM mass concentration of 15 % (Al_2O_3 + Al Graphite + Al and MgO + Al).

to other fluids. As illustrated in Fig. 15, since the temperature gains of the hybrid PCS based on Al_2O_3 + Al, MgO + Al and Graphite + Al are higher than the temperature gains of the hybrid PCS based on Al_2O_3, MgO and Graphite, it improves the thermal capacity of the collector by augmenting the photothermal conversion capacity of the collector. For instance, at volume concentration of 100 ppm and PCM mass concentration of 15/20 %, the temperature improvement of Graphite based PCS increases from 1.59 to 1.75 with the addition of Al nanoparticle. Likewise, the thermal energy storage augmentation boots from 4 to 4.4 at volume concentration of 100 ppm and PCM mass concentration of 20 %.

Furthermore, as seen in Fig. 16, hybrid PCS based on Al_2O_3 + Al, MgO + Al and Graphite + Al creates a more uniform temperature gradient than Al_2O_3, MgO and Graphite-based hybrid PCS by reducing the temperature differences inside the collector. Besides, the slurry starts to warm up from the collector base and the temperature of the slurry increases with the effect of free convection, moves upwards from the centre of the collector, and moves in the collector in the horizontal direction.

Moreover, it is seen in Fig. 17 that, since the heat generated by the irradiation decreases with the deepness of the solar cavity, the highest heat generation occurs at the vicinity of the upper plate. Further, the heat generation of the hybrid PCS based on Al_2O_3 + Al, MgO + Al and Graphite + Al is higher than the Al_2O_3, MgO and Graphite-based hybrid PCS with the benefit of Al nanoparticle additives, increasing the solar radiation absorption capacity.

5. Conclusions

Numerical heat transfer characteristics of a direct absorption solar collector using latent functional thermal fluid as the heat transfer fluid was carried out. These liquids, formed by the dispersion of nano-encapsulated nanoscale PCMs in the base fluid, are considered as a kind of new phase change slurry. The heat transfer and fluid flow characteristics were analysed in 2D employing ANSYS Fluent. The influences of PCM mass concentration, shell material type, core size and nanoparticle on the photothermal conversion behaviour of the latent functional

thermal fluid, were investigated. The findings unveiled that the thermal performance of PCS was better than that of the nanofluid. The solar thermal energy storage improvements of Cu, Al, Ag and Au nanofluids were 2.25, 2.06, 2.18 and 2.3, respectively, while the performances of PCS consisting of Al, Au, Ag and Cu-shelled paraffin core/shell structures were 3.49, 3.98, 4.21 and 4.19, respectively. In addition, the presence of free electrons in the metal surface layers created absorption peak positions by stimulating the surface plasmon resonance due to the interaction of the metallic shell materials with radiation. Besides, increasing the core diameter enhanced the overall size of the core/shell architecture, resulting in a decrease in the surface area-to-volume ratio of the capsule. It was found that the decreasing surface area-to-volume ratio caused agglomeration of the capsules, negatively affecting both the temperature and storage gains of the system. Furthermore, nanoparticles added to water were found to increase the performance of PCS. When the volume concentration was 25 ppm and the PCM mass concentration was 20 %, the heat storage improvements of the Al_2O_3, MgO and Graphite based PCS were 5.2, 5.14 and 4.8, respectively, while the Al_2O_3 + Al, MgO + Al and Graphite + Al hybrid PCS based PCS formed by the addition of Al nanoparticle's enhancements were 5.5, 5.46 and 5.21. Moreover, it is concluded that the solar radiation capture and absorption capacity can be increased in this system, where the latent functional thermal fluid can directly absorb solar energy, which uses it both as a working fluid and a storage medium. By this enhanced thermal performance, PCS can provide considerable advantages for photothermal conversion and storage applications by reducing dependence on carbon-based fuels.

CRediT authorship contribution statement

Oguzhan Kazaz: Conceptualization, Methodology, Software, Validation, Investigation, Formal analysis, Visualization, Writing – original draft, Writing – review & editing. **Nader Karimi:** Conceptualization, Supervision, Writing – review & editing. **Shanmugam Kumar:** Supervision, Writing – review & editing. **Gioia Falcone:** Supervision, Writing – review & editing. **Manosh C. Paul:** Conceptualization, Supervision, Writing – review & editing, Project administration, Resources, Funding acquisition.

Declaration of Competing Interest

The authors declare that they have no known competing financial interests or personal relationships that could have appeared to influence the work reported in this paper.

Data availability

Data will be made available on request.

Acknowledgments

The first author would like to thank the Turkish Ministry of National Education, Republic of Turkey for funding his PhD research study at the University of Glasgow.

References

[1] Q. Wang, Z. Dong, R. Li, L. Wang, Renewable energy and economic growth: New insight from country risks, Energy 238 (C) (2022), 122018.
[2] H. İçen, F.Y. Tatoğlu, The asymmetric effects of changes in price and income on renewable and nonrenewable energy, Renew. Energy 178 (2021) 144–152.
[3] A. Sohani, C. Cornaro, M.H. Shahverdian, M. Pierro, D. Moser, S. Nižetić, N. Karimi, L.K. Li, M.H. Doranehgard, Building integrated photovoltaic/thermal technologies in Middle Eastern and North African countries: Current trends and future perspectives, Renew. Sustain. Energy Rev. 182 (2023), 113370.
[4] "Global Energy and CO2 Status Report," International Energy Agency (IEA), 2019.
[5] "Special Report Global Warming of 1.5oC," Intergovernmental Panel on Climate Change (IPCC), 2018.
[6] A. Sohani, M.H. Shahverdian, H. Sayyaadi, S. Nižetić, M.H. Doranehgard, An optimum energy, economic, and environmental design based on DEVAP concept to reach maximum heat recovery in a PV-wind turbine system with hydrogen storage, Energ. Conver. Manage. 288 (2023), 117147.
[7] T. Güney, Solar energy, governance and CO2 emissions, Renew. Energy 184 (2022) 791–798.
[8] V. Khullar, H. Tyagi, N. Hordy, T.P. Otanicar, Y. Hewakuruppu, P. Modi, R. A. Taylor, Harvesting solar thermal energy through nanofluid-based volumetric absorption systems, Int. J. Heat Mass Transf. 77 (2014) 377–384.
[9] O. Kazaz, N. Karimi, S. Kumar, G. Falcone and M. C. Paul, "Effects of nanofluid's base fluid on a volumetric solar collector," in *11th International Conference on Renewable Power Generation - Meeting net zero carbon (RPG 2022)*, Hybrid Conference, London, UK, 2022.
[10] E.P.B. Filho, O.S.H. Mendoza, C.L.L. Beicker, A. Menezes, D. Wen, Experimental investigation of a silver nanoparticle-based direct absorption solar thermal system, Energ. Conver. Manage. 84 (2014) 261–267.
[11] C. Ho, K.-Y. Liu, T.-F. Yang, S. Rashidi, W.-M. Yan, Experimental study on cooling performance of water-based hybrid nanofluid with PCM and graphene nanoparticles, Case Stud. Therm. Eng. 33 (2022), 101939.
[12] O. Kazaz, K. N., G. Falcone, S. Kumar and M. C. Paul, "Effect of Radiative Heat Transfer in Nanofluid for Volumetric Solar Collector," in *13th International Conference on Applied Energy (ICAE2021)*, Thailand/Virtual, 2021.
[13] P. Raj, S. Subudhi, A review of studies using nanofluids in flat-plate and direct absorption solar, Renew. Sustain. Energy Rev. 84 (2018) 54–74.
[14] M. Hussain, S.K.H. Shah, U. Sajjad, N. Abbas, A. Ali, Recent Developments in Optical and Thermal Performance of Direct Absorption Solar Collectors, Energies 15 (19) (2022) 7101.
[15] A. Zeiny, H. Jin, L. Bai, G. Lin, D. Wen, A comparative study of direct absorption nanofluids for solar thermal applications, Sol. Energy 161 (2018) 74–82.
[16] H. Jin, G. Lin, L. Bai, M. Amjad, E.P.B. Filho, D. Wen, Photothermal conversion efficiency of nanofluids: An experimental and numerical study, Sol. Energy 139 (2016) 278–289.
[17] A. Lenert, E.N. Wang, Optimization of nanofluid volumetric receivers for solar thermal energy conversion, Sol. Energy 86 (1) (2012) 253–265.
[18] B. Liu, X. Zhang, J. Ji, Review on solar collector systems integrated with phase-change material thermal storage technology and their residential applications, Int. J. Energy Res. 45 (6) (2021) 8347–8369.
[19] C. Ho, C.-R. Siao, T.-F. Yang, B.-L. Chen, S. Rashidi, W.-M. Yan, An investigation on the thermal energy storage in an enclosure packed with micro-encapsulated phase change material, Case Stud. Therm. Eng. 25 (2021), 100987.
[20] C. Ho, K.-H. Lin, S. Rashidi, D. Toghraie, W.-M. Yan, Experimental study on thermophysical properties of water-based nanoemulsion of n-eicosane PCM, J. Mol. Liq. 321 (2021), 114760.
[21] E. Douvi, C. Pagkalos, G. Dogkas, M.K. Koukou, V.N. Stathopoulos, Y. Caouris, M. G. Vrachopoulos, Phase change materials in solar domestic hot water systems: A review, Int. J. Thermofluids 10 (2021), 100075.
[22] P. Charvát, L. Klimeš, O. Pech, J. Hejčík, Solar air collector with the solar absorber plate containing a PCM – Environmental chamber experiments and computer simulations, Renew. Energy 143 (2019) 731–740.
[23] M.A. Essa, N.H. Mostafa, M.M. Ibrahim, An experimental investigation of the phase change process effects on the system performance for the evacuated tube solar collectors integrated with PCMs, Energ. Conver. Manage. 177 (2018) 1–10.
[24] A. Kazemian, A. Salari, A. Hakkaki-Fard, T. Ma, Numerical investigation and parametric analysis of a photovoltaic thermal system integrated with phase change material, Appl. Energy 238 (2019) 734–746.
[25] F. Ran, Y. Chen, R. Cong, G. Fang, Flow and heat transfer characteristics of microencapsulated phase change, Renew. Sustain. Energy Rev. 134 (2020), 110101.
[26] Z. Qiu, X. Zhao, P. Li, X. Zhang, S. Ali, J. Tan, Theoretical investigation of the energy performance of a novel MPCM (Microencapsulated Phase Change Material) slurry based PV/T module, Energy 87 (2015) 686–698.
[27] Z. Qiu, X. Ma, X. Zhao, P. Li, S. Ali, Experimental investigation of the energy performance of a novel Micro-encapsulated Phase Change Material (MPCM) slurry based PV/T system, Appl. Energy 165 (2016) 260–271.
[28] M. Eisapour, A.H. Eisapour, M.J. Hosseini, P. Talebizadehsardari, Exergy and energy analysis of wavy tubes photovoltaic-thermal systems using microencapsulated PCM nano-slurry coolant fluid, Appl. Energy 266 (2020), 114849.
[29] Q. Yu, A. Romagnoli, R. Yang, D. Xie, C. Liu, Y. Ding, Y. Li, Numerical study on energy and exergy performances of a microencapsulated phase change material slurry based photovoltaic/thermal module, Energ. Conver. Manage. 183 (2019) 708–720.
[30] L. Liu, Y. Jia, Y. Lin, G. Alva, G. Fang, Performance evaluation of a novel solar photovoltaic–thermal collector with dual channel using microencapsulated phase change slurry as cooling fluid, Energ. Conver. Manage. 145 (2017) 30–40.
[31] Z. Wang, J. Qu, R. Zhang, X. Han, J. Wu, Photo-thermal performance evaluation on MWCNTs-dispersed microencapsulated PCM slurries for direct absorption solar collectors, J. Storage Mater. 26 (2019), 100793.
[32] B. Xu, C. Chen, J. Zhou, Z. Ni, X. Ma, Preparation of novel microencapsulated phase change material with Cu-Cu2O/CNTs as the shell and their dispersed slurry for direct absorption solar collectors, Sol. Energy Mater. Sol. Cells 200 (2019), 109980.
[33] J. Liu, L. Chen, X. Fang, Z. Zhang, Preparation of graphite nanoparticles-modified phase change microcapsules and their dispersed slurry for direct absorption solar collectors, Sol. Energy Mater. Sol. Cells 159 (2017) 159–166.
[34] ANSYS Fluent User's Guide, Canonsburg: ANSYS, Inc., 2013.

[35] H. Tyagi, P. Phelan, R. Prasher, Predicted Efficiency of a Low-Temperature Nanofluid-Based Direct Absorption Solar Collector, J. Sol. Energy Eng. 131 (4) (2009), 041004.
[36] C. F. Bohren and D. R. Huffman, Absorption and Scattering of Light by Small Particles, New York: Wiley, 1983.
[37] W. Lv, P.E. Phelan, R. Swaminathan, T.P. Otanicar, R.A. Taylor, Multifunctional Core-Shell Nanoparticle Suspensions for Efficient Absorption, J. Sol. Energy Eng. 135 (2) (2013), 021004.
[38] A.E. Neeves, M.H. Birnboim, Composite structures for the enhancement of nonlinear-optical susceptibility, J. Opt. Soc. Am. B 6 (4) (1989) 787–796.
[39] Y. Wu, L. Zhou, X. Du, Y. Yang, Optical and thermal radiative properties of plasmonic nanofluids, Int. J. Heat Mass Transf. 82 (2015) 545–554.
[40] S. Schelm, G.B. Smith, Evaluation of the limits of resonance tunability in metallic nanoshells with a spectral averaging method, J. Opt. Soc. Am. A 22 (7) (2005) 1288–1292.
[41] G.M. Hale, M.R. Querry, Optical Constants of Water in the 200-nm to 200-μm Wavelength Region, Appl. Opt. 12 (3) (1973) 555–563.
[42] E. D. Palik, Handbook of Optical Constants of Solids, Academic Press, 1997.
[43] M. Ma, Q. Ai, M. Xie, Optical properties of four types paraffin, Optik 249 (2022), 168277.
[44] S. Babar, J.H. Weaver, Optical constants of Cu, Ag, and Au revisited, Appl. Opt. 54 (3) (2015) 477–481.
[45] M.A. Ordal, L.L. Long, R.J. Bell, S.E. Bell, R.R. Bell, R.W. Alexander, C.A. Ward, Optical properties of the metals Al Co, Cu, Au, Fe, Pb, Ni, Pd, Pt, Ag, Ti, and W in the infrared and far infrared, Appl. Opt. 22 (7) (1983) 1099–1119.
[46] J. A. Duffie and W. A. Beckman, Solar Engineering of Thermal Processes, New Jersey: John Wiley & Sons, Inc., Hoboken, 2013.
[47] B. Chen, X. Wang, R. Zeng, Y. Zhang, X. Wang, J. Niu, Y. Li, H. Di, An experimental study of convective heat transfer with microencapsulated phase change material suspension: Laminar flow in a circular tube under constant heat flux, Exp. Therm Fluid Sci. 32 (8) (2008) 1638–1646.
[48] S.-H. Song, Q. Liao, W.-D. Shen, Laminar heat transfer and friction characteristics of microencapsulated phase change material slurry in a circular tube with twisted tape inserts, Appl. Therm. Eng. 50 (1) (2013) 791–798.
[49] M. Ghalambaz, A.J. Chamkha, D. Wen, Natural convective flow and heat transfer of Nano-Encapsulated Phase Change Materials (NEPCMs) in a cavity, Int. J. Heat Mass Transf. 138 (2019) 738–749.
[50] K. Khanafer, K. Vafai, M. Lightstone, Buoyancy-driven heat transfer enhancement in a two-dimensional enclosure utilizing nanofluids, Int. J. Heat Mass Transf. 46 (19) (2003) 3639–3653.
[51] P. Ternik, Conduction and convection heat transfer characteristics of water–Au nanofluid in a cubic enclosure with differentially heated side walls, Int. J. Heat Mass Transf. 80 (2015) 368–375.
[52] O.Z. Sharaf, A.N. Al-Khateeb, D.C. Kyritsis, E. Abu-Nada, Direct absorption solar collector (DASC) modeling and simulation using a novel Eulerian-Lagrangian hybrid approach: Optical, thermal, and hydrodynamic interactions, Appl. Energy 231 (2018) 1132–1145.
[53] M. Sheikholeslami, D.D. Ganji, H.R. Ashorynejad, Investigation of squeezing unsteady nanofluid flow using ADM, Powder Technol. 239 (2013) 259–265.
[54] W. Su, J. Darkwa, G. Kokogiannakis, Review of solid–liquid phase change materials and their encapsulation technologies, Renew. Sustain. Energy Rev. 48 (2015) 373–391.
[55] O. Kazaz, N. Karimi, S. Kumar, G. Falcone, M.C. Paul, Enhanced sensible heat storage capacity of nanofluids by improving the photothermal conversion performance with direct radiative absorption of solar energy, J. Mol. Liq. 372 (2023), 121182.
[56] O. Kazaz, N. Karimi, S. Kumar, G. Falcone, M.C. Paul, Effects of combined radiation and forced convection on a directly capturing solar energy system, Therm. Sci. Eng. Prog. 40 (2023), 101797.
[57] H. Mehling and L. F. Cabeza, Heat and cold storage with PCM: An Up To Date Introduction Into Basics and Applications, 2008.
[58] B.J. Lee, K. Park, T. Walsh, L. Xu, Radiative Heat Transfer Analysis in Plasmonic Nanofluids for Direct Solar Thermal Absorption, J. Sol. Energy Eng. 134 (2) (2012), 021009.
[59] T.P. Otanicar, P.E. Phelan, R.S. Prasher, G. Rosengarten, R.A. Taylor, Nanofluid-based direct absorption solar collector, J. Renew. Sustain. Energy 2 (3) (2010) 033102–033113.
[60] H.Y. Woo, D.W. Lee, T.Y. Yoon, J.B. Kim, J.-Y. Chae, T. Paik, Sub-100-nm Nearly Monodisperse n-Paraffin/PMMA Phase Change Nanobeads, Nanomaterials 11 (1) (2021) 1–9.
[61] S. Barlak, O.N. Sara, A. Karaipekli, S. Yapıc, Thermal Conductivity and Viscosity of Nanofluids Having Nanoencapsulated Phase Change Material, Nanoscale Microscale Thermophys. Eng. 20 (2) (2016) 85–96.
[62] F. Agresti, D. Cabaleiro, L. Fedele, S. Rossi, S. Barison, PMMA nano-encapsulated phase change material colloids for heat management applications, J. Mol. Liq. 377 (2023), 121576.
[63] S. Dugaria, M. Bortolato, D.D. Col, Modelling of a direct absorption solar receiver using carbon based nanofluids under concentrated solar radiation, Renew. Energy 128 (Part B) (2018) 495–508.
[64] M. Goel, S.K. Roy, S. Sengupta, Laminar forced convection heat transfer in microcapsulated phase change material suspensions, Int. J. Heat Mass Transf. 37 (4) (1994) 593–604.
[65] M.A. Ashraf, W. Peng, Y. Zare, K.Y. Rhee, Effects of Size and Aggregation/Agglomeration of Nanoparticles on the Interfacial/Interphase Properties and Tensile Strength of Polymer Nanocomposites, Nanoscale Res. Lett. 13 (214) (2018) 1–7.
[66] J. Li, L. Jia, L. Li, Z. Huang, Y. Chen, Hybrid Microencapsulated Phase-Change Material and Carbon Nanotube Suspensions toward Solar Energy Conversion and Storage, Energies 13 (17) (2020) 4401.